THE DESIGN AND SYNTHESIS OF FLUORESCENT CHEMOSENSORS FOR THE DETECTION OF GOLD AND MERCURY METAL SPECIES

A Thesis Submitted to
the Graduate School of Engineering and Sciences of
İzmir Institute of Technology
in Partial Fulfillment of the Requirements for the Degree of

MASTER OF SCIENCE

in Chemistry

by
Ceren CANTÜRK

June 2015
İZMİR

We approve the thesis of **Ceren CANTÜRK**

Examining Committee Members:

Assoc. Prof. Dr. Mustafa EMRULLAHOĞLU
Deparment of Chemistry, İzmir Institute of Technology

Prof. Dr. Mustafa Muammer DEMİR
Deparment of Materials Science and Engineering, İzmir Institute of Technology

Assist. Prof. Dr. Murat IŞIK
Deparment of Materials Science and Engineering, Bingöl University

16 June 2015

Assoc. Prof. Dr. Mustafa EMRULLAHOĞLU
Supervisor, Deparment of Chemistry,
İzmir Institute of Technology

Prof. Dr. Ahmet Emin EROĞLU
Head of the Deparment of Chemistry

Prof. Dr. Bilge KARAÇALI
Dean of the Graduate School of
Engineering and Science

ACKNOWLEDGEMENTS

There are a number of people who have assisted me during my graduate education. First of all, I would like to thank to my supervisor, Assoc. Prof. Dr. Mustafa Emrullahoğlu for his patience, encouragement and excellent guidance on the research which I performed. It was a pleasure for me to work in the field of fluorescent chemosensors and BODIPY chemistry, and it was honour to study with him.

Also I would like to thank to the members of research laboratory group, Muhammed ÜÇÜNCÜ, Erman KARAKUŞ, Ceyla ÇETİNTAŞ and Hüseyin ZEYBEK. Among these friends of mine, I would like to extend special thanks to Muhammed ÜÇÜNCÜ for his support, help, friendship and especially for his patience during three years. He was like a second brother to me and I am more than grateful for all of the things he has done for me.

Also, special thanks to Prof. Dr. Mustafa Muammer Demir and Assist. Prof. Dr. Murat Işık for participating as a committee member and reviewing my work and as well as Assist. Prof. Dr. Tuna Subaşı for HRMS analyses.

Endless gratitude is also extended to my parents, Hayri CANTÜRK and Necla CANTÜRK, my brother, Cumhur CANTÜRK and all my friends for providing love and support everytime that I got desperate. I love them very much.

Finally, I would especially like to thank to my beloved Egemen ŞENTÜRK for loving me unconditionally and for his everlasting encouragement.

ABSTRACT

THE DESIGN AND SYNTHESIS OF FLUORESCENT CHEMOSENSORS FOR THE DETECTION OF GOLD AND MERCURY METAL SPECIES

This study describes the design, synthesis and spectral behaviour of a fluorescent molecular sensor which is able to recognize Hg^{2+} and Au^{3+} ions via different emission modes.

Determination of identity and amount of heavy metal ions has crucial importance for scientific researches. Detection of trace metal ions can be achieved by classical spectroscopic methods such as atomic absorption and atomic emission spectroscopy and inductively-coupled plasma spectrometry. In contrast to these highly expensive and time consuming methods, fluorogenic or chromogenic methods provide an alternative way for the detection of these species. There are many organic molecules that act as signaling unit for fluorogenic sensing strategy such as rhodamine, fluorescein, coumarin and BODIPY derivatives. Among these, BODIPY fluorophore was chosen for this work as a signal reporter due to its unique properties.

In this research, the detection of Hg(II) and Au(III) ions was recognized in two distinct fluorescence changes: one resulting from a reversible Hg^{2+}/sensor complex formation, the other an irreversible Au^{3+}-mediated hydrolysis reaction. The minimum amount of Au(III) and Hg(II) ions detectable in aqueous solution was determined to be 128 nM and 160 nM, respectively. The capacity of the developed probe for imaging was studied in living cells. The investigation showed that the probe can be used efficiently for *in vitro* imaging of Au^{3+} and Hg^{2+} species.

ÖZET

ALTIN VE CİVA METAL BİLEŞİKLERİNİN TAYİN EDİLMESİ İÇİN FLORESAN ÖZELLİKTE KEMOSENSÖRLERİN TASARLANMASI VE SENTEZLENMESİ

Bu çalışmada Au(III) ve Hg(II) metal iyonlarının tayin edilebilmesi için floresan özellik gösteren BODIPY yapısında bir kemosensör tasarlanıp sentezlenmiş ve spektral özellikleri incelenmiştir.

Ağır ve geçiş metal iyonlarının tespiti için kemosensör tasarımı oldukça önemlidir. Çünkü bu iyonlar biyolojik sistemlerde önemli rol almakta ve buna karşın çevreye son derece toksik etkiler gösterebilmektedir. Bu iyonların tayini için atomik absorpsiyon ve atomik emisyon spektroskopisi, indüktif olarak eşleşmiş plazma spektrometresi gibi spektroskopik yöntemler kullanılabilir, ancak bu yöntemler karmaşık örnek hazırlama aşamaları ve sofistike cihazlar gerektirmektedir. Bu son derece pahalı ve zaman alıcı yöntemlerin yerine florojenik ve kromojenik yöntemler bu türlerin saptanması için iyi bir alternatif olabilir. Bilinen diğer floroforlara kıyasla sahip olduğu eşsiz özellikleriyle BODIPY floroforu metal iyon kemosensörü yapımı için oldukça iyi bir örnektir.

Bu tez çalışmasında Au^{3+} ve Hg^{2+} metal iyonlarının tayini iki farklı floresan değişimiyle gözlemlenmiştir. Hg(II) iyonlarının tayini tersinir Hg-sensör kompleks oluşumuna dayanırken, Au(III) iyonları tayini tek yönlü hidroliz reaksiyonu üzerinden gerçekleşmiştir. Yapılan ölçümler sonucunda sulu çözelti içerisinde tayin edilebilen en düşük Au^{3+} ve Hg^{2+} iyon miktarı sırasıyla 128 nM ve 160 nM olarak belirlenmiştir. Aynı zamanda, altın ve civa iyonlarına duyarlı olarak tasarlanan bu sensörün hücre içerisindeki aktivitesi de başarılı bir şekilde gösterilmiştir.

TABLE OF CONTENTS

LIST OF FIGURES

Figure **Page**

LIST OF ABBREVIATIONS

BODIPY	4, 4-difluoro-4-bora-3a, 4a-diaza-s-indacene
DDQ	2,3-Dichloro-5,6-dicyano-1,4-benzoquinone
TFA	Trifluoroacetic Acid
PET	Photoinduced Electron Transfer
THF	Tetrahydrofuran
DCM	Dichloromethane
DMF	Dimethyl Formamide
DCE	Dichloroethane
RT	Room Temperature
EtOH	Ethanol
DAPI	4',6-diamidino-2-phenylindole

CHAPTER 1

INTRODUCTION

1.1.An Overview

Today, determining the identity and amount of metal ions is a vital necessity in different areas of biochemistry, biotechnology, clinical diagnostics, materials science and environmental chemistry. With developing technology in recent years, there have been so many facilities for human beings in different areas of life. However, as an inevitable consequence of technological advances, environmental pollution has emerged. The potential risk of potable water and soil being contaminated with heavy metals in the form of industrial wastes threatens human health and the future of ecosystem. It is well known that heavy metal ions such as Hg^{2+}, Au^{3+}, Pb^{2+}, As^{3+} and Cd^{2+} are harmful and responsible for the rise of serious fatal diseases in human body. Especially Hg^{2+} ion has been considered to be the most toxic metal ion leading enviromental pollution over the others (Onyido et al., 2004). These heavy metal ions have no construction functions in human body and they are bioaccumulative. The accumulation of very low concentrations in organisms can even result in mortal consequences. Among these, mercury metal ion can lead to dysfunction of the brain, kidney and stomach. Because of the thiophilic nature of proteins and enzymes, the most affected part in human body is the central nervous system (Yang et al., 2009). On the other hand, gold ions are valid for the treatment of rheumatic, arthritis, tuberculosis and brain lesions. Unfortunately, overdose of these drugs used in the treatment of such diseases results in the interaction of gold ions with biomolecules including DNA and enzymes disturbing a series of cellular processes and leads to serious health problems (Do et al., 2010; Emrullahoglu et al., 2013). Consequently, the design of selective and sensitive methods has crucial importance in determining heavy metal ions in living cells.

Several techniques are available for this purpose including atomic absorption spectroscopy, inductively coupled plasma atomic emission spectroscopy and electrochemical sensoring. However, all of these methods need expensive equipment

and involve time consuming and inconvenient sample preparation steps. In addition, due to long preparation steps, there is a contamination possibility. As an alternative way, fluorometric and colorimetric techniques have become very popular since fluorescence measurements are very sensitive, easy to carry out, nondestructive and inexpensive. What is more, photophysical properties of a fluorophore can be adjusted by changing charge, electron and energy transfer (Quang et al., 2007). As a consequence of a need in the detection of metal ions, several articles about fluorescent chemosensors and chemodosimeters have been published.

The term chemodosimeter as a molecule providing analyte recognition with an irreversible transduction of an observable signal was first described by Czarnik and Chae in 1992 for the recognition of Hg(II) ions. In their research, they reported a fluorescent dosimeter that indicates mercury ions with fluorescence enhancement in aqueous solution (Chae et al., 1992). Their work offered an insight into other studies.

1.2.BODIPY Fluorophore

Within the classes of fluorescent dyes, 4, 4-difluoro-4-bora-3a, 4a-diaza-s-indacene, usually known as BODIPY, has recently attracted great attention and its popularity has risen in a very short period of time. The first boron dipyrrin dye was synthesized by Treibs and Kreuzer in 1968 (Treibs et al., 1968). They discovered that the acylation of 2,4-dimethylpyrrole, **1**, with acetic anhydride and boron trifluoride as being Lewis acid catalyst, produced a highly fluorescent compound **4**. Acid catalyzed condensation of pyrroles **1** and **2** resulted in to dipyrrin, **3**, and complexation with a boron trifluoride generated dye **4** (Figure 1.1).

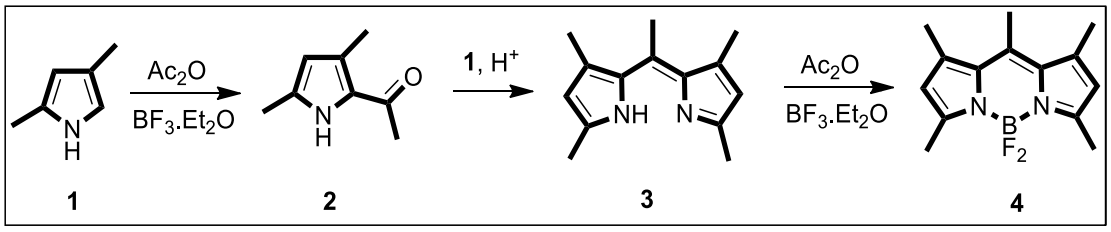

Figure 1.1. First synthesis of a boron dipyrrin dye by Treibs and Kreuzer (Source: Boens et al., 2012)

There are many remarkable features of BODIPY fluorophore. Robustness against light and chemicals, relatively high molar absorption coefficients and high

fluorescence quantum yields, narrow emission bandwidths with high peak intensities, good solubility, resistance towards self-aggregation in solution, stability in physiological pH range and excitation/emission wavelengths in the visible spectral region (≥ 500 nm) could all arouse interest in these compounds (Boens et al., 2012). Apart from this, the spectroscopic and photophysical properties of this fluorophore can be adjusted by attaching residues at the appropriate positions of BODIPY core.

IUPAC numbering system of a boron dipyrrin compound is described in Figure 1.2. The central carbon is called as the meso position of the core. Moreover, the positions adjacent to nitrogen atoms are called α-positions that indicate the reactivity of this positions in pyrroles, and the others are β-positions.

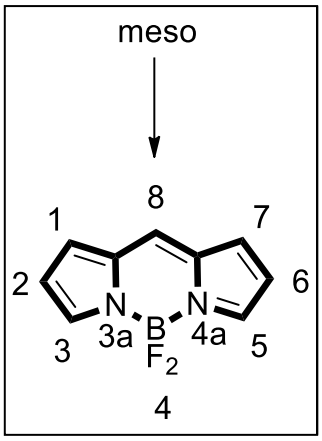

Figure 1.2. IUPAC numbering system of a boron dipyrrin compound
(Source: Wood et al., 2007)

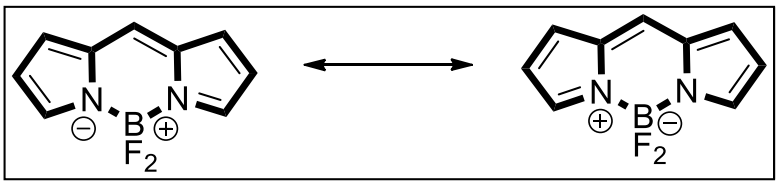

Figure 1.3. Delocalized structures of BODIPY with formal charges

Synthesis routes for borondipyrromethene core mainly proceed from porphyrin chemistry (Wood et al., 2007). Acid catalyzed condensation of aldehyde **6** with pyrrole **5**, in which unsubstituted pyrroles are used as a solvent to avoid polymerization (Littler et al., 1999) produces dipyrromethane, **7**, compounds (Figure 1.4). On the other hand, for 2-substituted pyrroles, an excess amount of pyrrole is not needed because multiple

condensations are not competing side reaction. Dipyrromethane compounds are very sensitive to light and air, and they have a very low stability. For this reason, after they are prepared, it is better to use them immediately. Oxidation of dipyrromethane, **7**, with DDQ or p-chloranil results in to dipyrrin, **8**. Besides, in very few cases where the aldehyde is not an aromatic aldehyde, oxidation tends to fail (Wood et al., 2007). When the oxidation is complete, allowing dipyrrin, **8**, to react with base and boron trifluoride etherate yields the boron difluoride complex **9**.

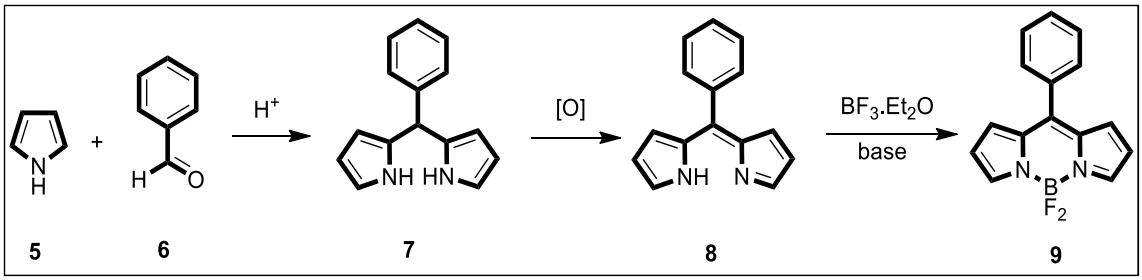

Figure 1.4. Acid catalyzed condensation of aromatic aldehydes with pyrroles (Source: Boens et al., 2012)

There is a different method to procure boron difluoride complexes. It includes the condensation of pyrrole, **5**, with an acylium derivative **10 (**Figure 1.5). An acylium derivative could be an acid anhyride (Li et al., 2006), an acid chloride (Shah et al., 1990), or an ortho-ester (Yakubovskyi et al., 2009). With the advantage of this route prodiving us to have asymmetric dipyrrins, an isolated acylpyrrole can be allowed to react with the second pyrrole moiety **5b** in an acidic condensation. And treating **12** with an excess base and boron trifluoride etherate generates BODIPY dye **13**.

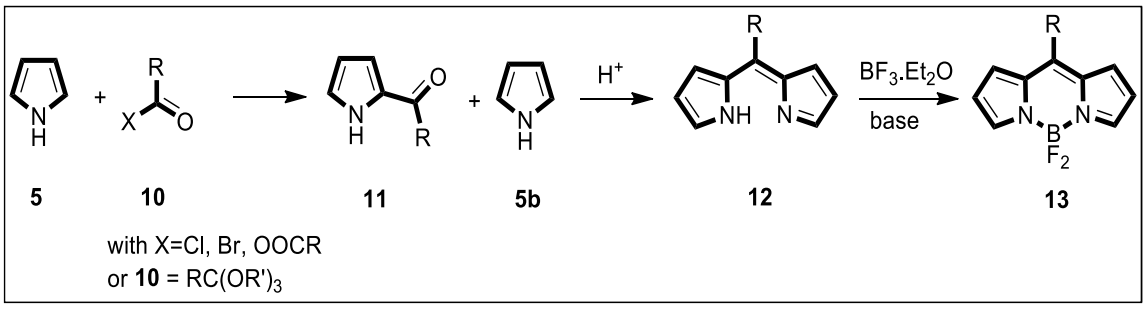

Figure 1.5. Synthesis of BODIPY dyes with the acylation of pyrrole followed by condensation and complexation (Source: Boens et al., 2012)

Instead of the condensation of an acylated pyrrole, the last alternative for the synthesis of BODIPY dyes was described by Wu and Burgess in 2008 (Wu et al., 2008).

They serendipitously discovered that without the second equivalent of pyrrole, the same product can be prepared from the aldehyde alone. This is because phosphorus oxychloride has the power of condensing pyrrole-2-carbaldehyde, **14**, by itself without a second need in pyrrole. When phosphorus oxychloride is replaced with another Lewis acid like TFA or $BF_3.Et_2O$, the dipyrromethenium cation formation did not take place (Figure 1.6).

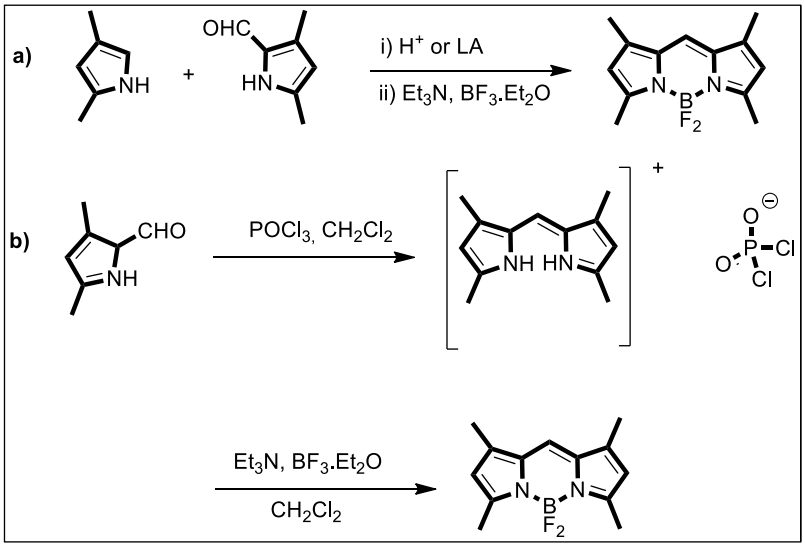

Figure 1.6. (a) Conventional synthesis of tetramethyl-BODIPY and (b) the new approach described (Source: Wu et al., 2008)

In the reaction mechanism, the aldehyde oxygen is replaced with chlorine atom resulting in a chlorinated azafulvene, **16**, by phosphorus oxychloride. It proceeds with the nucleophilic attack by chloride anion and decomposition of unstable intermediate **17** generates a dipyrrin, **19** (Figure 1.7). Clearly, this mechanism is only possible for 5-substituted pyrrole aldehydes.

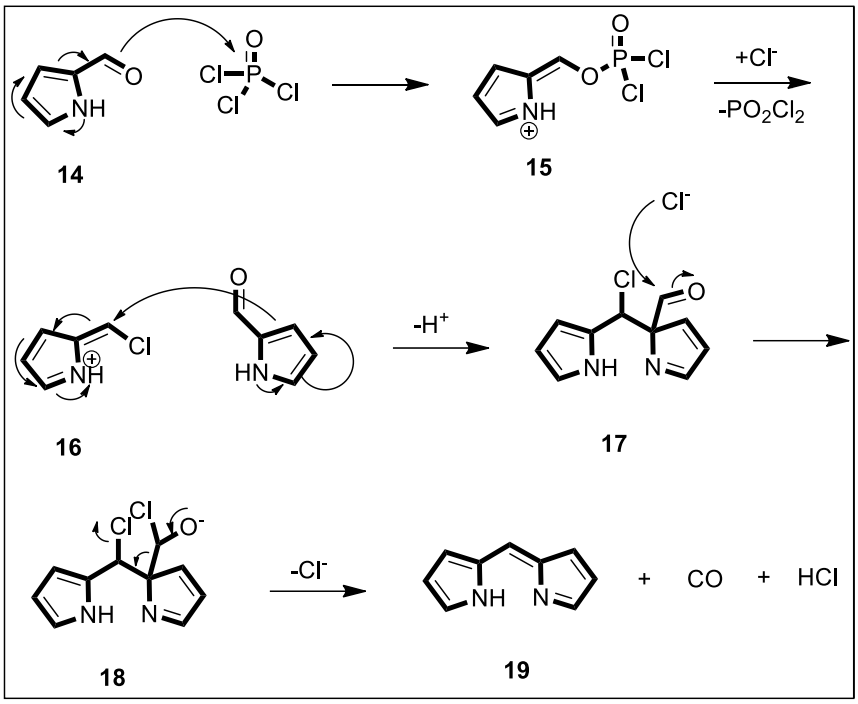

Figure 1.7. A possible mechanism for the formation of dipyrromethene (Source: Wu et al., 2008)

Earlier, it was mentioned that the photophysical and spectroscopic properties of BODIPY can be changed by the attachment of different residues at the appropriate positions. When alkyl groups are attached to BODIPY core in the way of **21**, spectral properties are not affected significantly. Compounds **20** and **21** both have high fluorescence (φ_f=0.93, φ_f =0.80) (Schmitt et al., 2009). However, introduction of an aryl group to meso position, **22**, results in an important decrease in quantum yield of fluorescence (Leen et al., 2011). The reason for that is assigned to the rotation of the aryl group acting as a nonfluorescent material. In order to fix the rotation of the aryl group, methyl residues can be subjected to the core at the positions 1,7 to obtain a significant increase in quantum yield of fluorescence of dye **23** (Figure 1.8) (Gabe et al., 2004).

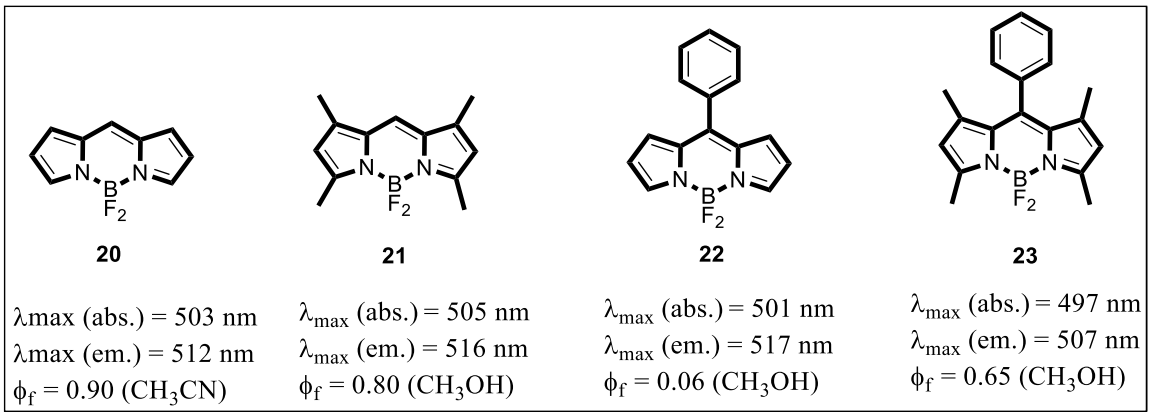

Figure 1.8. Influence of alkyl and meso aryl substituents on the spectroscopic properties

Among the factors that have an influence on the spectroscopic properties of BODIPY, conjugation has a substantial importance. By increasing the conjugation, the colour of the dye can be shifted to the red region. This is handily accomplished by introducing aryl groups in to the system, **24** (Verbelen et al., 2012). But, as long as aryl groups are free to rotate in space, the red shift is weakened. On such systems, fixing the rotation of the aryl groups can still increase the quantum yield of fluorescence. What is more, enlargement of the conjuation with larger aromatic systems or alkene or alkyne groups, **25** (Huang et al., 2012) shifts the absorption and emission maxima of the dyes even further to the red (Figure 1.9).

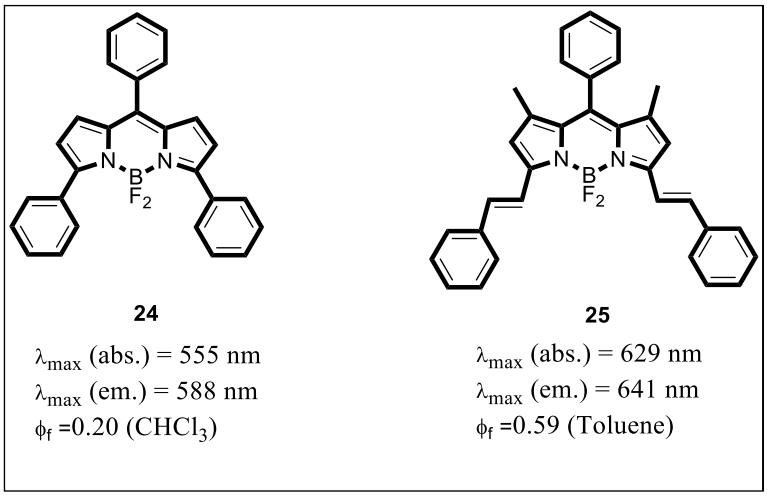

Figure 1.9. Influence of extended conjugation on the spectroscopic properties

The BODIPY chromophore can be easily modified by introducing heteroatoms directly to the core. Such modification has similar effects with the one above. The 8-thiomethylated dye **26** (Leen et al., 2012) has absorption and emission maxima on the

red region, and this also accounts for a 3-sulfur substituted dye **27** (Rohand et al., 2006) and dye **28** (Rohand et al., 2006). Aryl group at the meso position is again responsible for lowering the quantum yield (Figure 1.10).

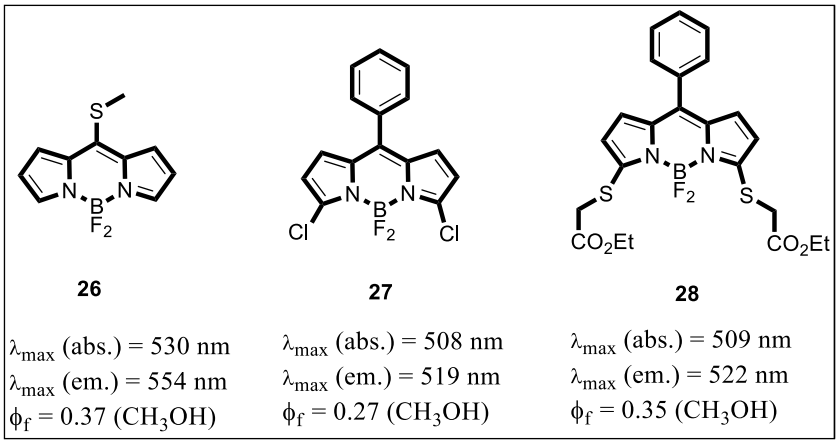

Figure 1.10. Influence of electron donating nucleophiles on the spectroscopic properties

Besides the distinctive properties of BODIPY, the fact that it could be modified according to the purpose of use is the reason why this dye has a significantly large field of application. Some of these application fields are photodynamic therapy (Ozlem et al., 2009), dye sensitized solar cells (Barin et al., 2009), molecular logic gates (Bozdemir et al., 2010), ion sensing (Bozdemir et al., 2010), and light harvesting system (Figure 1.11).

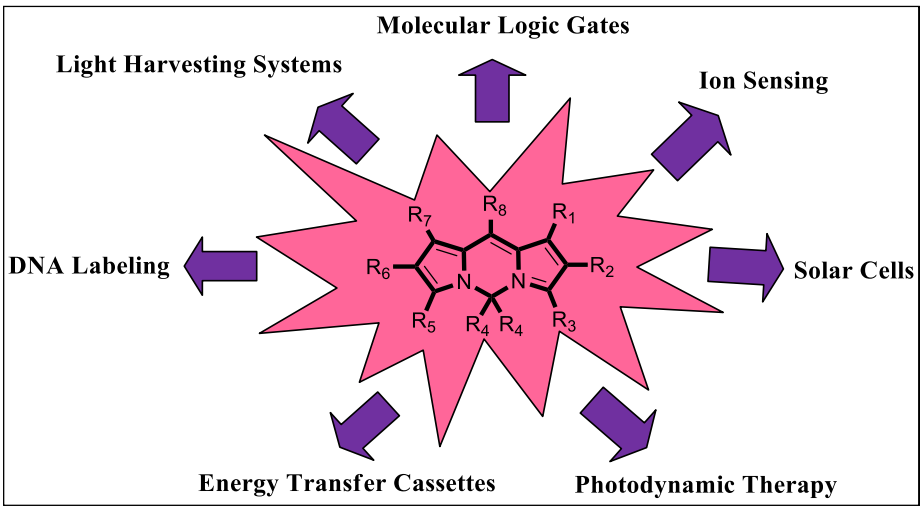

Figure 1.11. Application fields of BODIPY dyes

1.3. Literature Studies Published on Gold Sensing Probes

Lately, the detection of gold ions has attracted great attention. As a consequence of this, plenty of studies were reported. The first gold ion selective fluorescent chemosensor was described by Yang and his co-workers in 2009 (Yang et al., 2009). In their study, they developed an irreversible fluorescent probe that shows no selectivity to other metal ions and whose mechanism was based on a cyclization reaction of a rhodamine amide with an alkyne group. Due to the strong alkynophilicy of gold ions, they have the power to activate the cyclization of the alkynes (Cho et al., 2009; Dujols et al., 1997). When rhodamine amide with an alkyne moiety was activated with gold ions, spirocyclic ring opening reaction of rhodamine took place (Figure 1.12). As a result of this, the molecule started to fluoresce very strongly.

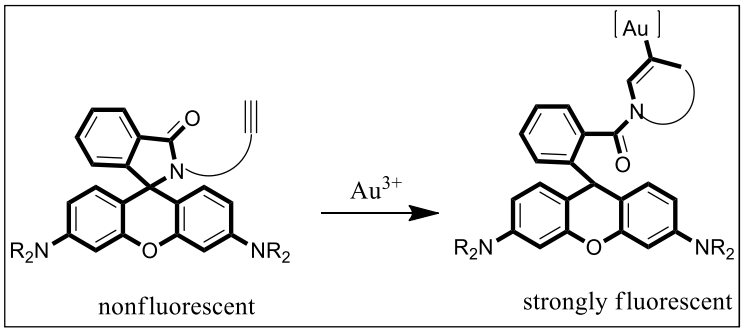

Figure 1.12. Reaction-based fluorescent sensing of gold ions
(Source: Yang et al., 2009)

Approximately 50 nM of Au^{3+} ions could be detected in aqueous media with the developed probe. To detect the reversibility of the probe, excess amounts of CN^- ions were conducted to the solution to release gold cyanide complexes; however, no decrease was observed in the fluorescence intensity. Although they could not isolate the resulting reaction product, acetylene proton peak seemed to have disappeared in the ^{1}H-NMR spectrum. Therefore, the process was considered to be irreversible. As the last work of the study, bioimaging applications were conducted by using HeLa cells.

In the upcoming times of 2009, another gold selective chemodosimeter was reported. Jou et al. published the first off-on fluorescent probe for Au^{3+} that was based on a cyclization of a propargyl amide (Jou et al., 2009). Lately, rhodamine derivatives has been used in so many studies. In this work, rhodamine dye was functionalized with an alkyne moiety to give a fluorescence change (Figure 1.13).

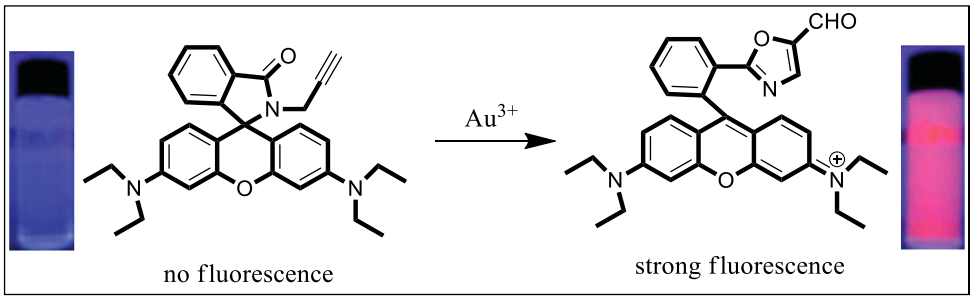

Figure 1.13. Au^{3+}-induced transformation from propargylamide to oxazolecarbaldehyde (Source: Jou et al., 2009)

The fluorescence change was assigned to the ring opening spirolactam followed by intramolecular cyclization reaction forming oxazolecarbaldehyde. Detection limit of the probe was estimated to be 63 ppb. For the detection of gold(III) ions in living cells, HaCaT cell line was cultured.

Compared to year 2009, much more studies were published in 2010. One of them was developed by Egorova et al. which was based on a rhodamine-derived alkyne (Egorova et al., 2010). A fluorescence sensing system for Au(I)/Au(III) species was designed for the first time based on their alkynophilicity (Figure 1.14). In the presence of Au(I)/Au(III), spirolactam ring opening reaction and consequent heterocycle formation upon coordination with gold ions took place. And sensing process resulted in both color and fluorescence changes. As a major reaction product in aqueous media, 5-formyloxazole which was identified in $^{1}H/^{13}C$ NMR and MS data was formed. Formyloxazole was possibly formed from vinylgold intermediate by gold-promoted hydration and concomitant double reductive elimination processes. The detection limit of the developed probe for AuCl was determined to be 0.4 ppm.

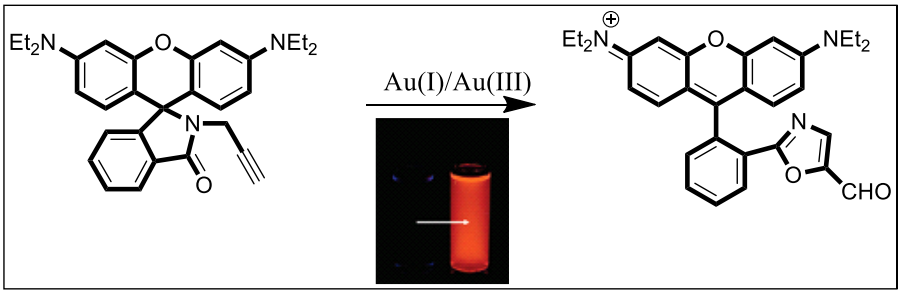

Figure 1.14. Au(I)/Au(III)-promoted sensing process (Source: Egorova et al., 2010)

Much later in 2010, Do and his co-workers reported a study with a similar sensing mechanism from the papers mentioned above (Do et al., 2010). They designed a fluorophore to yield a strong fluorescence change through a gold ion-mediated hydroarylation reaction. According to the proposed mechanism, fluorophore derived from apocoumarin was activated with gold(III) ions based on the strong alkynophilicy of gold ions. Then, with a concomitant intramolecular electrophilic aromatic substitution, hydroarylation reaction was completed (Figure 1.15). The fluorescent reaction product was identified with $^{1}H/^{13}C$ NMR and MS analysis. And the detection limit of the probe for Au(III) ions in protic solvents was determined to be 64 ppb. As the last work of the paper, fluorescent microscopic imaging studies were performed by using HaCaT cells.

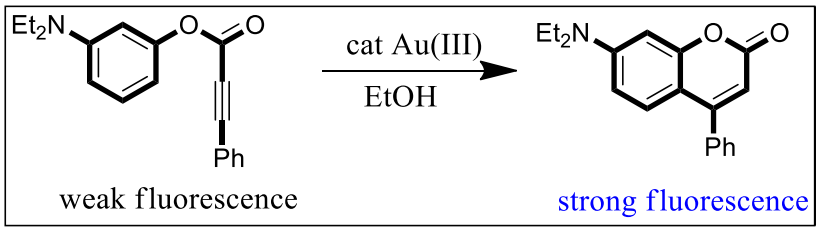

Figure 1.15. Response of the developed probe towards Au(III) species
(Source: Do et al., 2010)

Towards the end of 2010, a study different from all of the work mentioned above was reported by Dong et al. (Dong et al., 2010). They designed a probe based on 1,8-naphtalimide and alkyne conjugate for the ratiometric sensing of Au^{3+} and Hg^{2+} by adjusting pH in aqueous solutions (Figure 1.16). This study enlightens the selective detection of two different metal ions in aqueous solutions with a significant fluorescence change. Mechanistic analysis of the probe for the recognition of both Au^{3+} and Hg^{2+} was based on Kucherov reaction. In the presence of mentioned ions, a short lived π complex occurred and was attacked by water with Markovnikov regioselectivity and antistereoselectivity. The resulting vinyl gold intermediate was then converted to methyl ketone. Obtained reaction products were isolated and characterized by $^{1}H/^{13}C$ NMR and mass spectrometry. The detection limit of the probe was determined to be 10 ppb.

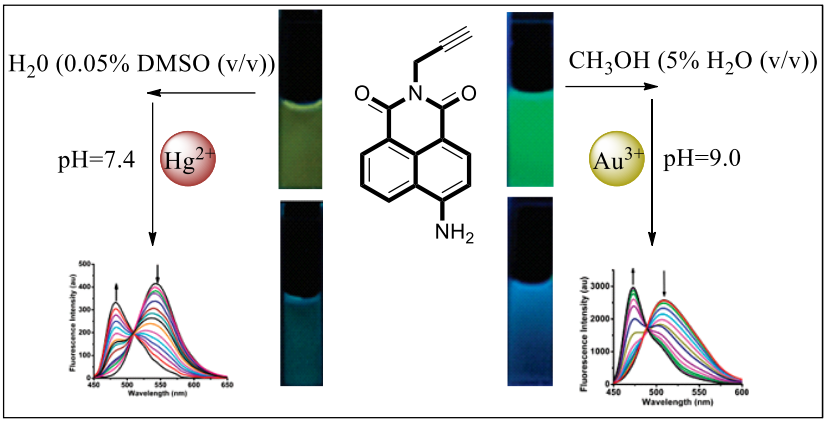

Figure 1.16. Ratiometric fluorecent sensing of Au^{3+} and Hg^{2+} (Source: Dong et al., 2010)

As it was mentioned earlier, although rhodamine derivatives were preferred more often than BODIPY-derived molecules in gold sensing based studies, a good example was published in 2012 by Wang and his co-workers (Wang et al., 2012). In their study, they developed a fluorescent BODIPY-based probe for the detection of Au(III)/Au(I) through blocking photoinduced electron transfer. The synthesized BODIPY derivative was a nonfluorescent compound owing to photoinduced electron transfer from the aniline unit to the BODIPY moiety. But, when it was treated with Au(III)/Au(I), 2'-ethynyl biphenylamine unit was transformed to the phenanthridine moiety by intramolecular hydroamination. The loss of electron donating amino group blocked PET process. As a result, the molecule started to fluoresce very strongly (Figure 1.17).

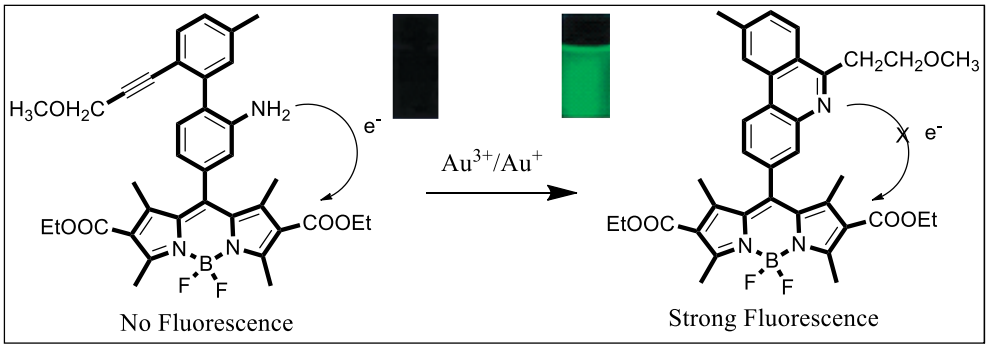

Figure 1.17. Hydroamination of the developed probe in the presence of Au^{3+}/Au^{+} (Source: Wang et al., 2012)

Based on the recorded data, the detection limit of the developed probe was determined to be 320 nM. And fluorescence microscopic imaging for Au(III) was

conducted with HeLa cells. This work provided new ideas for designing fluorescent probes for gold ions.

In the following years, a new approach, anchoring-unanchoring of a fluorophore, was described by Patil et al. for the detection of gold ions (Patil et al., 2012). In this approach, the fluorescence of fluorophore was quenched by anchoring with an organic substrate. By the interaction with gold ions, highly fluorescent molecule was released from the probe with the formation of organic product (Figure 1.18).

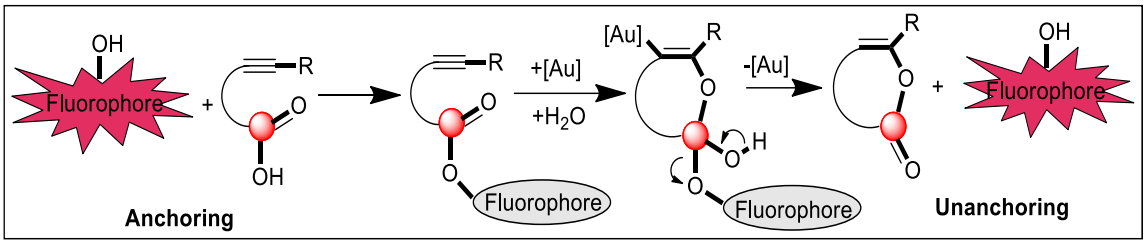

Figure 1.18. Approach involving anchoring-unanchoring of a fluorophore (Source: Patil et al., 2012)

Bioimaging studies were performed with A549 lung cancer cells. It was believed that this study could allow biodegradable fluorescent probes for cancer diagnostics in the future.

Lately in 2013 and 2014, our research group developed three gold selective fluorescent probes. As it was mentioned before, due to their strong affinity to alkynophilic metals, alkynes are favorable binding platforms for gold ions. In one of our studies, rhodamine dye was functionalized with an alkyne moiety to give a significant fluorescence change (Emrullahoglu et al., 2013). The overall sensing process was determined to be reaction based. When Au^{3+} ions were subjected to the solution, gold-mediated intramolecular cyclization and consequent ring opening reaction took place to generate highly fluorescent isoquinoline rhodamine derivative (Figure 1.19). To detect the reversibility of the developed probe, excess amount of CN^- ions were released to the solution. However, no change was observed in either fluorescence or color. Due to this observation, the sensing process was determined to be an irreversible process. As the last work of the study, human colon carcinoma cells (HCT 116) were cultured to record fluorescence images in the presence of Au^{3+} ions.

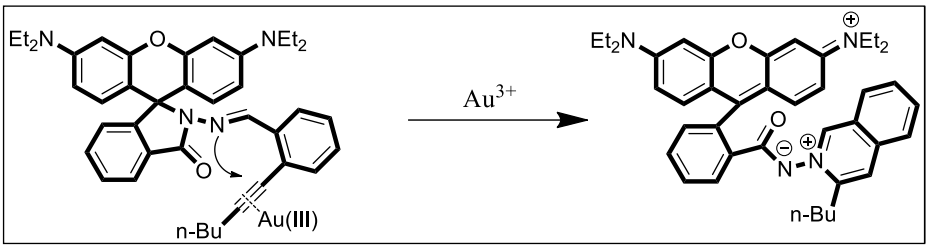

Figure 1.19. Proposed reaction mechanism of Au(III) sensing process (Source: Emrullahoglu et al., 2013)

In the following study of ours, two different fluorophores, rhodamine and BODIPY, were integrated with each other through C=N double bond for the first time allowing the differential detection of Hg^{2+} and Au^{3+} (Karakus et al., 2014). Both fluorophores were nonemissive before the addition of any metal species. The C=N double bond in BODIPY unit blocked the BODIPY emission because of a non-radiative deactivation process of the excited state through a rapid isomerization of the C=N group. And rhodamine unit was nonemissive since it existed in the ring closed form. When the molecule was excited at 525 nm in the presence of Au^{3+} ions, a new emission band that belonged to the ring opened isomer of rhodamine core was obtained. On the other hand, when the same molecule was excited at 470 nm, a different emission band which was a characteristic emission band of BODIPY fluorophore was observed. The additon of Hg^{2+} ions to the solution led to the ring opened derivative of rhodamine. However, when the probe solution was excited at 470 nm in the presence of Hg(II) ions, no emission bands were recorded which meant that BODIPY was still in its off mode (Figure 1.20). The bioimaging applications of the developed probe were constructed with A549 lung adenocarcinoma cell lines.

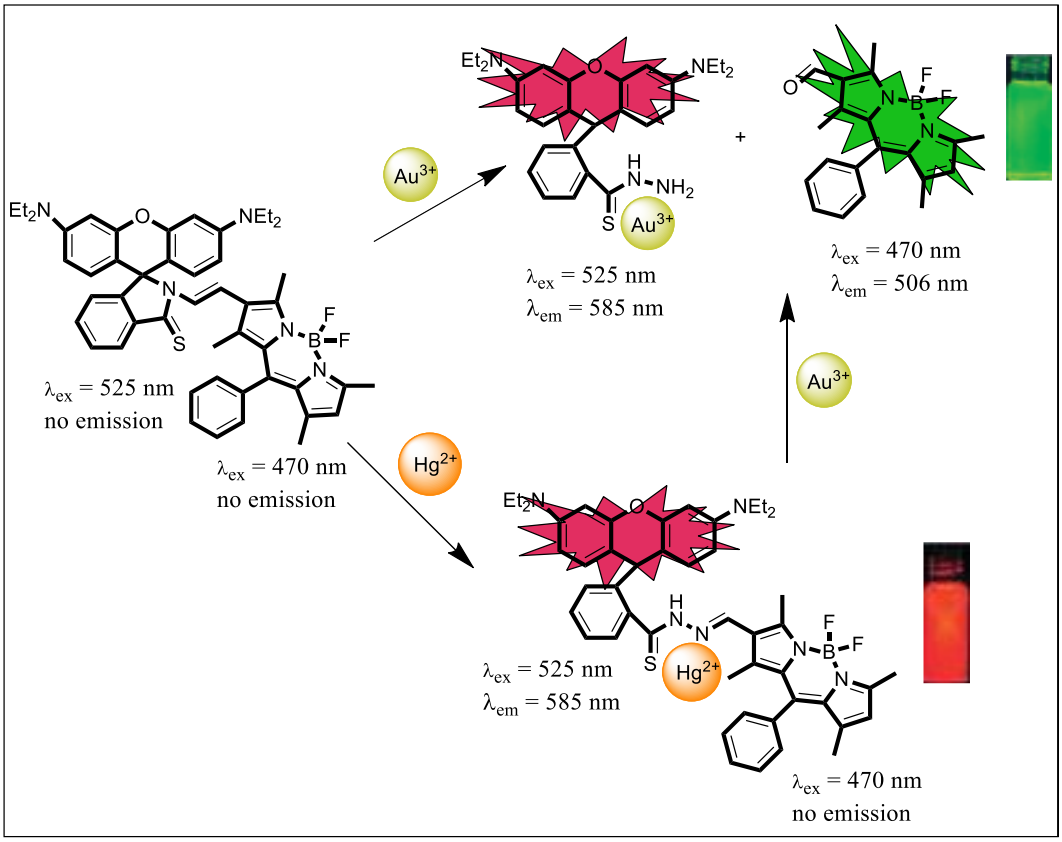

Figure 1.20. Response of the developed probe to the additon of Hg^{2+} and Au^{3+} (Source: Karakus et al., 2014)

1.4. Literature Studies Published on Mercury Sensing Probes

In literature, there are considerably more mercury selective sensors compared to gold sensing probes. Taking into consideration that mercury is one of the most toxic heavy metals in environment, such researches are quite valuable. Metal ions such as Hg(II), Pb(II), Cu(II) and Fe(III) often cause fluorescence intensity to decrease by quenching the fluorescence due to paramagnetic effects (Fabbrizzi et al., 1994). However, chemodosimetric approach allows us to design "turn on" fluorescent probes for the quenching of these heavy metals.

The first mercury selective probe was described by Czarnik and Chae who also defined the term dosimeter for the first time in 1992 (Chae et al., 1992). In their research, anthracene fluorophore was functionalized with thioamide group. Isomerization of C=S double bond often causes the molecule to exist in the thiolate form. And it is well known that thiolate structures are readily oxidized and they quench the fluorescence intensity of dye molecules through photoinduced electron transfer

mechanism. However, when Hg^{2+} ions were subjected into aqueous solution of the molecule, thioamide form was converted to the amide structure, and PET process was no longer effective. Consequently, the molecule started to fluoresce very strongly (Figure 1.21). The sensing process of the developed probe was irreversible and because of that it was called as chemodosimeter for the first time in scientific community. Following this pioneering work, many exciting papers have been published by using different fluorophores.

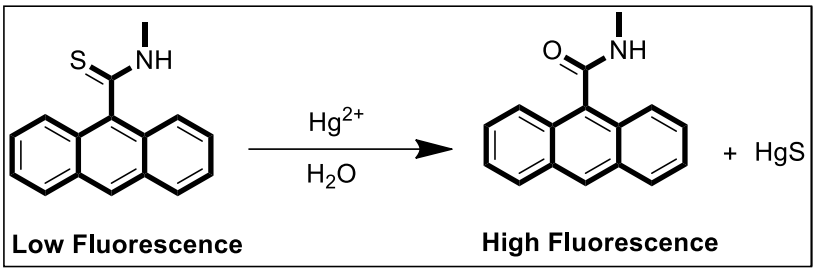

Figure 1.21. Response of the developed probe with the addition of Hg^{2+} (Source: Chae et al., 1992)

Later on, in order to develop a technique for the determination of Hg(II) ion, Tae and his co-workers designed a novel chemodosimeter in 2005 (Yang et al., 2005). In this paper, they took advantage of the spirolactam ring opening process and Hg(II)-mediated 1,3,4-oxadiazole cyclization of the thiosemicarbazide (Figure 1.22). The reaction was monitered by colorimetric as well as fluometric intensity changes at room tempereature in a 1:1 stoichiometric ratio to the amount of Hg^{2+}. The developed probe showed no selectivity to the other metal ions. Although small fluorescence enhancements appeared with the addition of Ag(I) and Zn(II), these metal ions did not interfere with the Hg(II)-induced fluorescence response. The detection limit of the probe was evaluated to be in parts per billion level.

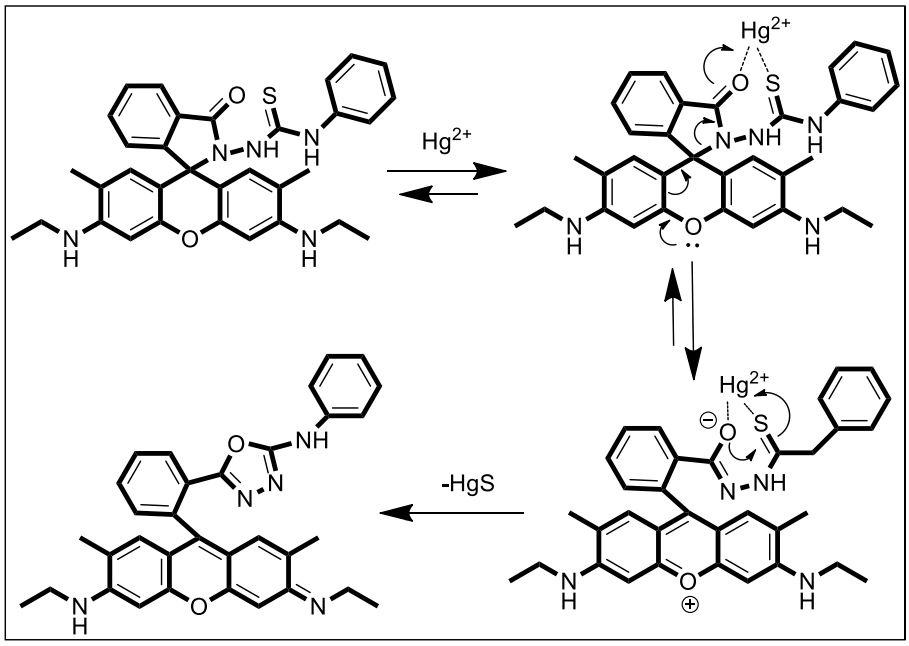

Figure 1.22. Hg^{2+}-induced ring opening and cyclization of the designed rhodamine derivative (Source: Yang et al., 2005)

At the very beginning of 2007, Wu et al. designed a similar Hg(II) selective fluorescent and colorimetric chemodosimeter (Wu et al., 2007). They developed N-(Rhodamine-6G)lactam-N'-phenylthiourea-ethylenediamine as a fluorescent and colorimetric chemodosimeter in an aqueous solution with a broad pH range (Figure 1.23). The design of the probe was based on the well known reaction of thiourea derivatives with amine resulting into guanidine derivatives with the subjection of Hg^{2+} ions into the solution. In the presence of Hg^{2+} ions, desulfurization reaction took place and consequent ring opening of spirolactam of rhodamine occurred. The subsequent intramolecular guanylation was the last step of the sensing mechanism. Introduction of Hg^{2+} ions also resulted in the color change from blue to yellow which was observable with the naked eye. Other metal ions showed no fluorescence and absorbance change and did not interfere with the Hg(II)-induced response. This proved that spirocyclic ring opening and consequent guanylation process was very selective for Hg(II) ions.

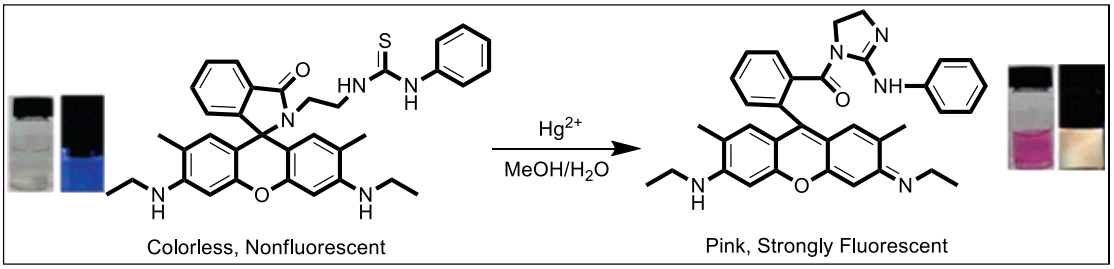

Figure 1.23. Response of the developed probe to the addition of Hg(II) ions (Source: Wu et al., 2007)

Another valuable work was published by Akkaya and his co-workers in the year 2007 (Coskun et al., 2007). They have reported the first application of aryl-substituted boratriazaindacenes in ratiometric metal ion sensing. The emission peak of the developed probe was at 682 nm at the determined solvent. When mercury ion was introduced into the solution, an isobestic point of 672 nm was observed and the formed mercury complex had a red-shifted emission peak at 719 nm. The dissociation constant was determined to be 5.4×10^{-6} M with a 1:1 binding stoichiometry. It has been seen before that when electronwithdrawing groups exist on the fluorophore π-system and involved in cation binding, charge separated excited-state is more stabilized than the ground state, thus energy gap is reduced. In this article, 2-pyridyl substituents interact with mercury ions in this way producing the observed bathochromic shift in the spectrum (Figure 1.24).

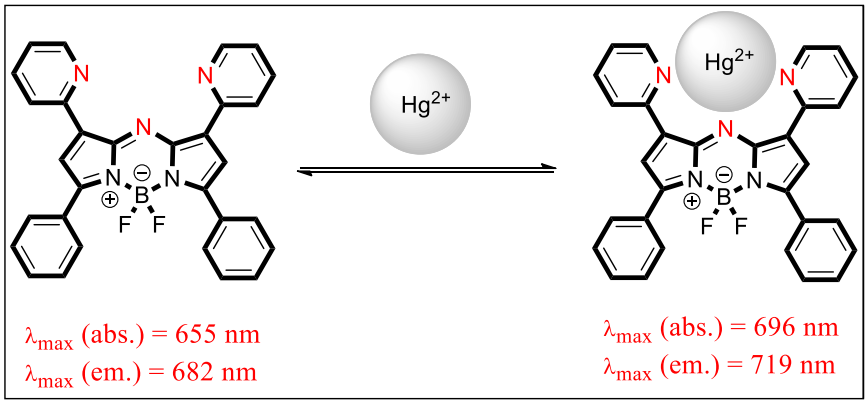

Figure 1.24. Hg^{2+}-induced response of modified boratriazaindacene (Source: Coskun et al., 2007)

By now, all of the mercury sensing probes explained so far have been based on the increase or decrease in the fluorescence intensity at a single emission wavelength. A

different study apart from these was described by Shang et al. in 2008 (Shang et al., 2008). In this work, fluorescein fluorophore was linked to rhodamine B hydrazide through a thiourea spacer for the selective ratiometric detection of Hg^{2+} ions. When Hg(II) ions were introduced into a solution, spirolactam ring opening process took place resulting in the release of fluorescent rhodamine B moiety. Afterwards, an intramolecular fluorescence resonance energy transfer (FRET) from fluorescein to rhodamine occurred (Figure 1.25). In the free form of the developed probe, fluorescein chromophore exhibited a single emission band at 520 nm when excited at 490 nm. In the presence of mercury(II) ions, different emission band at 591 nm corresponding to the ring opened form of rhodamine moiety was noted. With the addition of increasing amounts of Hg(II), a decrease in fluorescence intensity at 520 nm and a concominant increase in fluorescence intensity at 591 nm were observed. It was concluded that the reaction stoichiometry of the probe for Hg(II) was 1:1 and the detection limit was determined to be 0.05 μM.

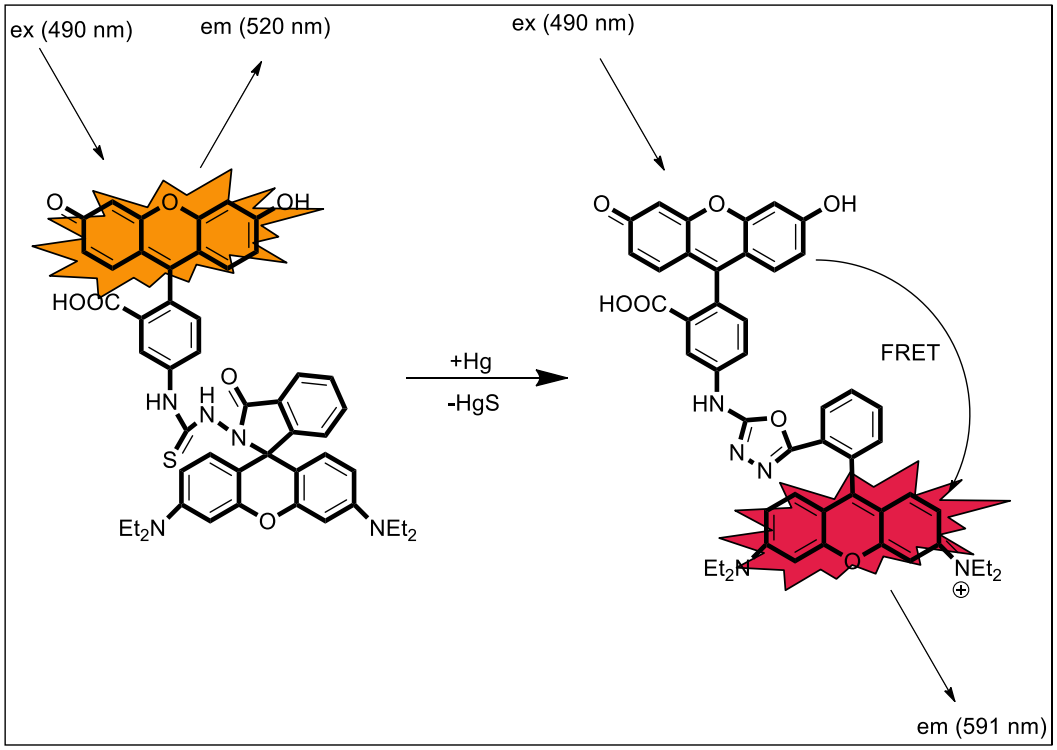

Figure 1.25. FRET-based detection mechanism of Hg^{2+}
(Source: Shang et al., 2008)

In 2009, Fan et al. designed a fluorescent chemosensor containing a BODIPY fluorophore and carboxyl-thiol metal bonding moieties that is selective towards Hg^{2+}

over other metal ions (Figure 1.26) (Fan et al., 2009). The molecule had no fluorescence intensity without the addition of any metal ions due to the photoinduced electron transfer from receptor to the BODIPY fluorophore. With the introduction of Hg^{2+} ions, the fluorescence intensity increased by over 123-fold with a 1:1 binding stoichiometry. The dissociation constant and the detection limit of the probe were determined to be $5.0\pm0.4\times10^{-6}$ M and 77 nM, respectively. To evaluate the selectivity of metal binding properties, many alkali and alkaline cations were used and none of them showed any response. To detect the reversibility of the system, excess amounts of NaI were added to the solution. 50% of the fluorescence emission intensity was quenched indicating that the sensing process could be reversible. As the last work of the study, bioimaging applications were conducted by using PC12 cell lines.

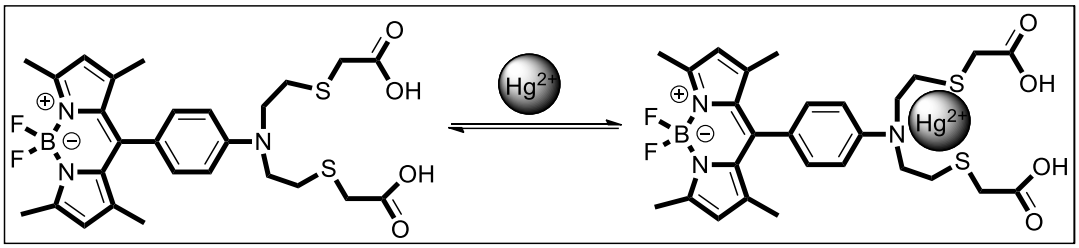

Figure 1.26. Sensing mechanism towards the addition of Hg^{2+}
(Source: Fan et al., 2009)

A different selective Hg(II) sensing method by coupling the internal charge transfer to excitation energy transfer with large Stokes shift was developed by Akkaya and his co-workers in the year 2010 (Figure 1.27) (Atilgan et al., 2010). Their main goal was to push the absorption and the emission wavelengths to the red/near IR region by using the known BODIPY chemistry together with Huisgen type click chemistry. Without the addition of any metal ions, there were two clear emission peaks at 518 and 725 nm. However, when mercury ions were subjected, a blue shift in the emission spectrum occurred with the increment of the intensity. Also a decrease in the emission intensity of the shorter wavelength was observed representing the increased energy transfer due to the larger spectral overlap, as the mercury ions strongly bound to the dithiaazacrown ligand. Later, they made the titration of the chemosensor with Hg(II) ions and while shorter wavelength peak did not change, longer wavelength peak was shifted hypsochromically providing an isobestic point at 662 nm. For the free chemosensor, the emission lifetime was determined to be 3.0 ns but when mercury ions

were present, the lifetime decreased to 1.8 ns. Corresponding energy transfer efficiencies were 11% and 45%, respectively.

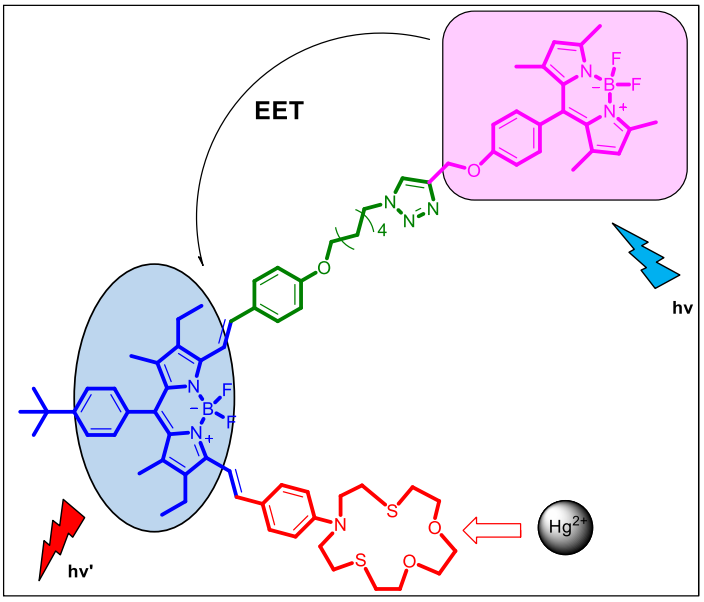

Figure 1.27. Selective Hg(II) sensing by coupling the internal charge transfer to excitation energy transfer (Source: Atılgan et al., 2010)

At the beginning of 2011, a new hydrazone derivative groups was synthesized by Kim et al. for the selective detection of Hg(II) ions in microfluidic systems (Kim et al., 2011). To achieve this, two new chemosensors were designed one containing thiol group and the other one carboxylic acid group. Both of the chemosensors were in their off state without the addition of any metal ions. The ring opening process of spirolactam caused the colorimetric and fluorimetric changes in the presence of Hg^{2+} ions and none of the other metal ions generated any changes. For the chemosensor bearing thiol group, there was 2:1 binding stoichiometry between the chemosensor and Hg^{2+} (Figure 1.28) and its detection limit was determined to be 1 nM. For the other chemosensor containing carboxylic acid group, 1:1 binding stoichiometry was observed between the chemosensor and Hg^{2+} (Figure 1.28) and its detection limit was determined to be 4.23 nM. As the last work of the study, *in vivo* imaging of mercury ions in *C.elegans* was conducted.

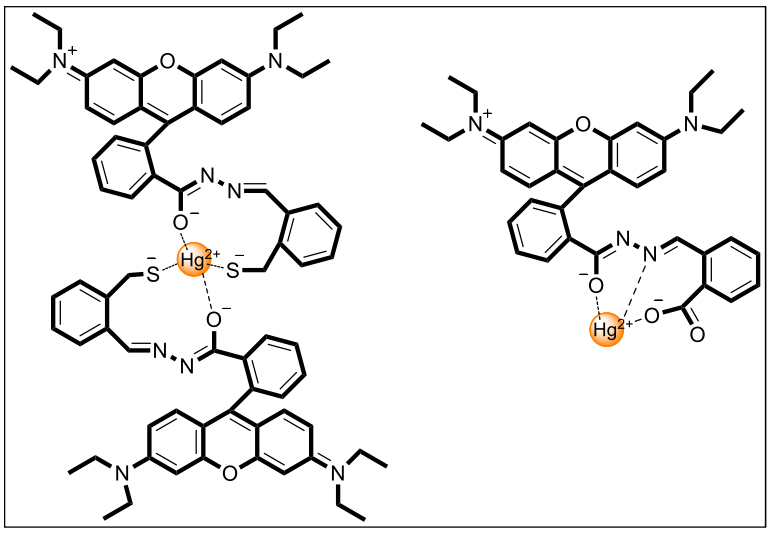

Figure 1.28. Proposed binding modes of the developed two chemosensors containing thiol and carboxylic acid groups (Source: Kim et al., 2011)

In year 2014, Bera et al. designed a rhodamine-rhodanine based turn on fluorescent chemosensor and described its application in living cells as well as in a living vertebrate organism (Bera et al., 2014). They theorized that the introduction of 3-aminorhodanine to a rhodamine based probe would increase its affinity towards Hg^{2+} ion by anchoring the thiosulphamide bond with Hg^{2+}. The reaction mechanism was based on the spirolactam ring opening process leading cyclizations and insertion of Hg^{2+} to the formed seven-membered ring, which was cleaved, and formation of water soluble mercury complex (Figure 1.29). The process was determined to be irreversible considering the formation of 1,3,4-oxadiazole ring. The probe was proved to detect the presence of 0.5 pM concentration of Hg^{2+}. For *in vivo* detection of mercury ions were evaluated in HeLa, HEK293T (somatic cell), RN46A (serotonergic neuronal cell line), midbrain-derived MN9D (dopaminergic neuronal cell line), and rat primary cortical neuronal cultures.

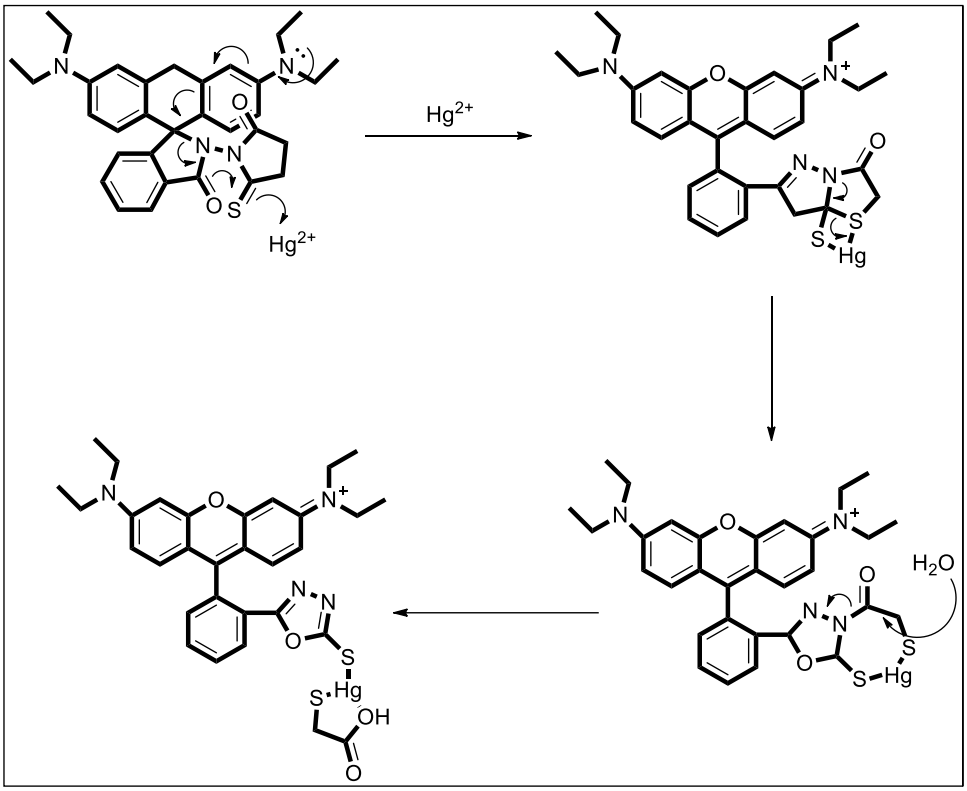

Figure 1.29. Proposed sensing mechanism of Hg^{2+}
(Source: Bera et al., 2014)

CHAPTER 2

EXPERIMENTAL STUDY

2.1.General Methods

All reagents were purchased from commercial suppliers (Aldrich and Merck) and used without further purification. ^{1}H NMR and ^{13}C NMR were measured on a Varian VNMRJ 400 Nuclear Magnetic Resonance Spectrometer. UV absorption spectra were obtained on Shimadzu UV-2550 Spectrophotometer. Fluorescence measurements were performed by using Varian Cary Eclipse Fluorescence spectrophotometer. Samples were put in quartz cuvettes with a path length of 10.0 mm (2.0 mL volume). Upon excitation at 460 nm, the emission spectra were integrated over the range 480 nm to 750 nm. The slit width was 5 nm for both excitation and emission. Melting points were determined by using an Electrothermal Melting Point Apparatus 9200. pH was recorded by HI-8014 instrument (HANNA). All measurements were conducted at least in triplicate.

2.2.Synthesis Section

The synthesis pathway for BOD-ZN was shown in Figure 2.1. BOD-1 and BOD-AL were synthesized according to the literature procedure (Emrullahoğlu et al., 2013). BOD-1 was converted to its aldehyde form by using the well known Vilsmeier Haack's formylation reaction. By using appropriate hydrazine hydrate, phenyl isothiocyanate and catalytic amount of acetic acid in methanol, BOD-ZN was synthesized (Cunha et al., 2009).

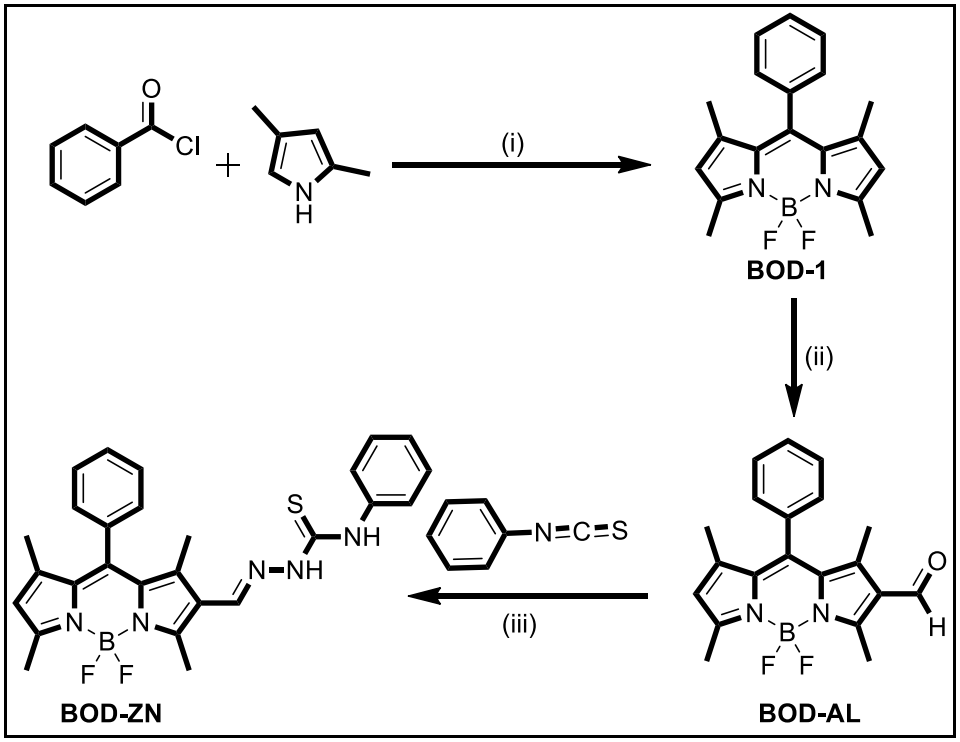

Figure 2.1. Synthesis pathway of BOD-ZN. (i) DCM, RT, overnight, then Et_3N and BF_3OEt_2 (ii) $POCl_3$, DMF, 0°C, then DCE, 60°C, overnight, (iii) Hydrazine hydrate, phenyl isothiocyanate, methanol, reflux

2.2.1.Synthesis of BOD-1

To a solution of 2,4-dimethylpyrrole (600 µL, 6 mmol) in CH_2Cl_2 (25 mL), benzoyl chloride (300 µL, 3 mmol) was added. The mixture was stirred at room temperature overnight, then after the addition of triethylamine (3 mL), $BF_3.OEt_2$ (3 mL) was added dropwise to the mixture which was cooled with an ice bath. The mixture was stirred again at room temperature overnight, then extracted with CH_2Cl_2 (100 mL). Combined organic phases were dried over anhydrous $MgSO_4$ and evaporated under reduced pressure. The crude product was purified by column chromotagraphy (10:1 Hexane:Ethyl Acetate) to afford BOD-1 as an orange-yellow solid (180 mg, 23% yield) (Wu et al., 2011). ^{1}H NMR (400 MHz, $CDCl_3$) δ: 7.49-7.47 (m, 3H), 7.28-7.26 (m, 2H), 5.98 (s, 2H), 2.55 (s, 6H), 1.37 (s, 6H). ^{13}C NMR (100 MHz, $CDCl_3$) δ: 155.40, 143.15, 141.72, 134.95, 129.13, 128.93, 127.90, 121.19, 14.59, 14.34.

Another alternative procedure for the synthesis of BOD-1 also exists. According to this procedure, into a solution of benzaldeyhde (400 µL, 4 mmol) and 2,4-dimethylpyrrole (800 µL, 8 mmol) in THF (25 mL), several drops of trifluoroacetic acid

were added. The mixture was stirred at room temperature overnight and then a solution of DDQ (910 mg, 4 mmol) in THF (30 mL) was added. The mixture was kept stirring for another 4 h. After triethylamine (12 mL) was added, $BF_3.OEt_2$ (12 mL) was injected dropwise to the mixture which was cooled with an ice bath. The mixture was again stirred at room temperature overnight and then extracted with CH_2Cl_2 (100 mL). Organic portion was washed with 5% $NaHCO_3$ solution (100 mL) and then with water. Afterwards, combined organic phases were dried over $MgSO_4$ and they were purified by column chromatography (10:1 Hexane:Ethyl Acetate) to afford BOD-1 as an orange-yellow solid (500 mg, 43% yield) (Liu et al., 2008).

2.2.2.Synthesis of BOD-AL

Into dry DMF (250 µL, 3.2 mmol) under ice bath (0 ^oC), $POCl_3$ (250 µL, 2.7 mmol) was added drop by drop. The mixture was stirred at room temperature for 40 min. Afterwards, BOD-1 (81 mg, 0.25 mmol) in DCE (10 mL) was added dropwise into the the mixture and the mixture was kept stirring at 60^oC at overnight. At the end of the reaction, the mixture was extracted with iced-$NaHCO_3$ solution (100 mL) and CH_2Cl_2 (100 mL). Combined organic phases were dried over $MgSO_4$ and they were purified with column chromatography (4:1 Hexane:Ethyl Acetate) to afford BOD-AL as orange solid (52.1 mg, 60% yield) (Isik et al., 2013). ^1H NMR (400 MHz, $CDCl_3$) δ: 10.0 (s, 1H), 7.53-7.51 (m, 3H), 7.28-7.26 (m, 2H), 6.15 (s, 1H), 2.81 (s, 3H), 2.61 (s, 3H), 1.64 (s, 3H), 1.41 (s, 3H). ^{13}C NMR (100 MHz, $CDCl_3$) δ: 185.92, 161.64, 156.45, 147.32, 143.55, 142.89, 134.12, 129.49, 127.67, 126.28, 124.01, 15.09, 14.85, 13.03, 11.55.

2.2.3.Synthesis of BOD-ZN

To a mixture of BOD-AL (52.1 mg, 0.15 mmol) and hydrazine hydrate (12 µL, 0.18 mmol) in 5 ml of methanol, phenyl isothiocyanate (23 µL, 0.18 mmol) was injected. Then, a drop of glacial acetic acid was added and the resulting solution was refluxed for an hour. After cooled down to room temperature, the solvent was removed under reduced pressure. The resultant residue was purified by column chromatography (10:1 (Hexane:Ethyl acetate)) to afford BOD-ZN as purple solid (29.4 mg, 40 % yield) (Cunha et al., 2009). Mp: 228-231 ^oC. ^1H NMR (400 MHz, $CDCl_3$) δ: 9.92 (s, 1H), 8.95

(s, 1H), 7.97 (s, 1H), 7.60 (d, J=8.0 Hz, 2H), 7.52-7.51 (m, 3H), 7.36 (t, J=8.0 Hz, 2H), 7.28-7.26 (m, 2H), 7.21 (t, J=7.2 Hz 1H), 6.09 (s, 1H), 2.75 (s, 3H), 2.59 (s, 3H), 1.50 (s, 3H), 1.40 (s, 3H). ^{13}C NMR (100 MHz, $CDCl_3$) δ: 174.7, 159.4, 153.9, 145.9, 142.5, 139.6, 138.1, 137.9, 134.5, 133.0, 130.5, 129.4, 128.7, 127.9, 125.9, 123.9, 123.1, 122.1, 14.9, 14.7, 14.1, 12.5.

CHAPTER 3

RESULTS AND DISCUSSION

In this study, a new molecular sensor with a single fluorophore based on a BODIPY dye appended with semithiocarbazone functionality as the metal recognition motif was developed. Based on previous studies in our laboratory, we had the knowledge of the affinity of thiourea motif towards Hg(II) ion. It is known from literature that most molecular sensors devised for mercury ions use sulphur moieties as recognition unit. Another challenging point taken into consideration while designing the probe was the existence of C=N functionality that plays an important role in sensing of Au(III) ion. In the light of these considerations, the fluorophore core was designed to be inactive in its initial state yet expected to become active in response to the mentioned metal species. The investigation started with the evalution of the optical behaviour of BOD-ZN in different solvents. So, different solvent systems such as EtOH/Phosphate buffer solution (v/v, 1:1, pH = 7.0), CH_3CN/Hepes buffer solution (v/v, 1:1, pH = 7.0) and DMSO/Phosphate buffer solution (v/v, 1:100, pH = 7.0) were examined for BOD-ZN to response Au^{3+} and Hg^{2+} metal ions. The highest increment in fluorescence intensity was observed in EtOH/Phosphate (v/v, 1:1, pH = 7.0) solvent system for both Au^{3+} and Hg^{2+}. At this point, it was necessary to evaluate the effect of the fraction of water to the spectral behaviour of BOD-ZN. For the next step, different ratios of EtOH and 0.1 M Phosphate buffer solution were examined. And, it was clearly seen that when the molecule is excited at 460 nm, 0.1 M Phosphate buffer/EtOH (v/v, 1:4, pH = 7.0) system gave the best result for the sensing of both Au^{3+} and Hg^{2+} (Figure 3.1 and 3.2). However, as shown in Figure 3.1 and Figure 3.2, 0.1 M Phosphate buffer/EtOH (v/v, 1:9, pH = 7.0) system gave higher fluorescence intensity than 0.1 M Phosphate buffer/EtOH (v/v, 1:4, pH = 7.0) solvent system. Despite this, 0.1 M Phosphate buffer/EtOH (v/v, 1:4, pH = 7.0) solution was decided to be used in this study because of the applicability of the probe to the cell imaging. On the other hand, it is significant to mention when CH_3CN/Hepes buffer solution was used as a solvent, the similar emission spectra were observed but the reproducibility of the results were less pronounced in this solvent system.

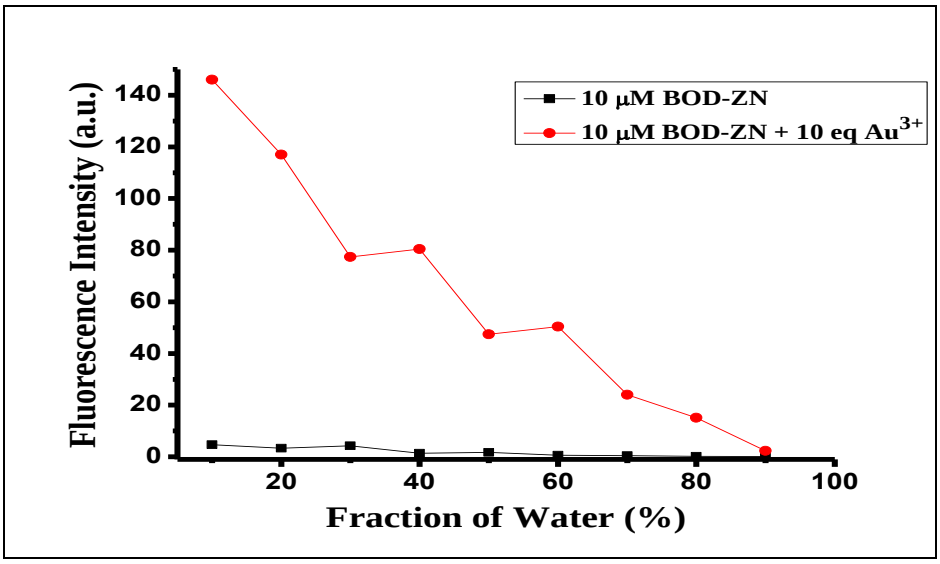

Figure 3.1. Effect of fraction of water on the fluorescence intensity of BOD-ZN (10 μM) in 0.1 M phosphate buffer/EtOH (pH = 7.0) in the absence and presence of Au^{3+} (10.0 equiv., 100 μM) (λ_{ex} = 460 nm, λ_{em} = 480 nm)

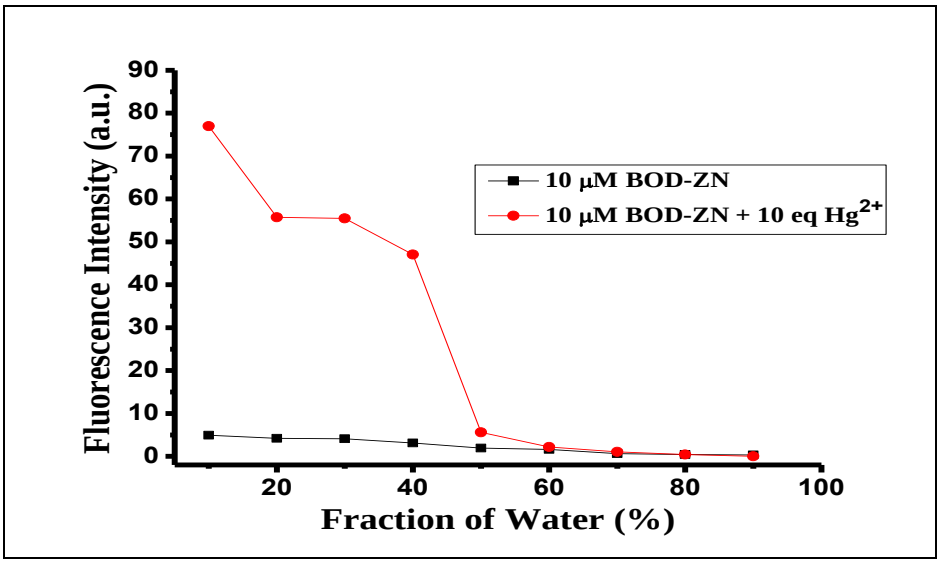

Figure 3.2. Effect of fraction of water on the fluorescence intensity of BOD-ZN (10 μM) in 0.1 M phosphate buffer/EtOH (pH = 7.0) in the absence and presence of Hg^{2+} (10.0 equiv., 100 μM) (λ_{ex} = 460 nm, λ_{em} = 480 nm)

After 0.1 M Phosphate buffer/EtOH (v/v, 1:4) was determined to be the solvent system, the effect of pH to the fluorescence intensity was surveyed. For Au^{3+} ion, pH 2, 3 and 4 caused a very slight increase in the fluorescence intensity. In other words, the probe did not work well in acidic media. As it can be seen from Figure 3.3, the greatest increment was observed at pH 8. For Hg^{2+}, basic media gave better results than acidic media, too (Figure 3.4). The fluorescence intensity at pH 10 was observed to be the

highest. However, since cell imaging studies are affected by a pH value different than body pH, it was decided to perform the studies at a pH of 7.

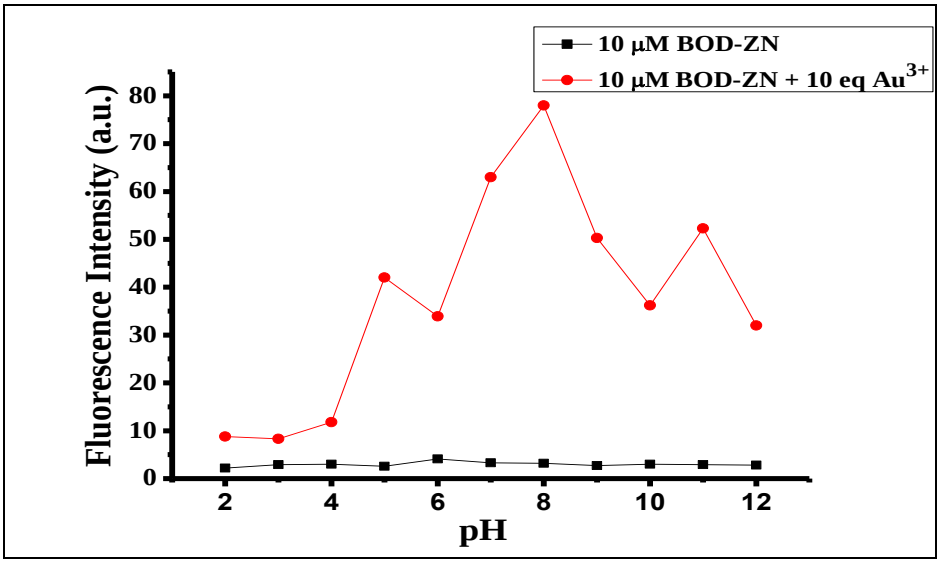

Figure 3.3. Effect of pH on the fluorescence intensity of BOD-ZN (10 μM) in 0.1 M phosphate buffer/EtOH (v/v, 1:4) in the absence and presence of Au^{3+} (10.0 equiv., 100 μM) (λ_{ex} = 460 nm, λ_{em} = 480 nm)

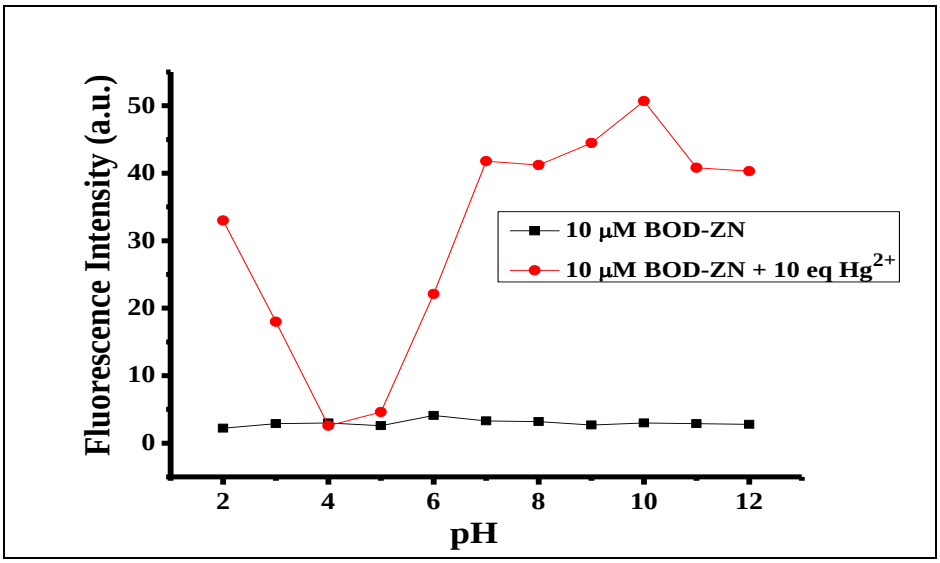

Figure 3.4. Effect of pH on the fluorescence intensity of BOD-ZN (10 μM) in 0.1 M phosphate buffer/EtOH (v/v, 1:4) in the absence and presence of Hg^{2+} (10.0 equiv., 100 μM) (λ_{ex} = 460 nm, λ_{em} = 480 nm)

Investigation was continued with the evaluation of the optical behaviour of BOD-ZN to the addition of various metal ions. As shown in Figure 3.5, BOD-ZN showed no significant spectral response to the metal ions such as Cu^{2+}, Ag^{+}, Zn^{2+}, Pb^{2+},

Ni^{2+}, Na^{+}, Mg^{2+}, Li^{+}, I^{-}, Pd^{2+}, Fe^{3+}, F^{-}, Cd^{2+}, Ca^{2+}, Ba^{2+}, Au^{+}, and Cr^{3+}, except for Hg^{2+} and Au^{3+}. Surprisingly, while the Au(III) ion enhances the fluorescence intensity, the Au(I) ion did not turn on the fluorescence even though 20 equiv. of AuCl was added to BOD-ZN solution. This is possibly due to a significant interaction between the more highly charged Au(III) ion and the probe compared to Au(I) ion.

One of the most significant characteristics of being a good sensor is to have minimum interference with other metal species present in the cell and that no change of signal is observed as a result of any possible interaction. Having clarified the detection of both metal species, the interference of other metal ions in the detection of Au^{3+} and Hg^{2+} was assessed. Although the spectral response of BOD-ZN induced by Au^{3+} ions showed no remarkable interference with other metal ions (Figure 3.6), the detection of Hg^{2+} was a little bit disturbed in the presence of Ca^{2+} and Cd^{3+}, but the detection of Hg(II) ion was not affected (Figure 3.7).

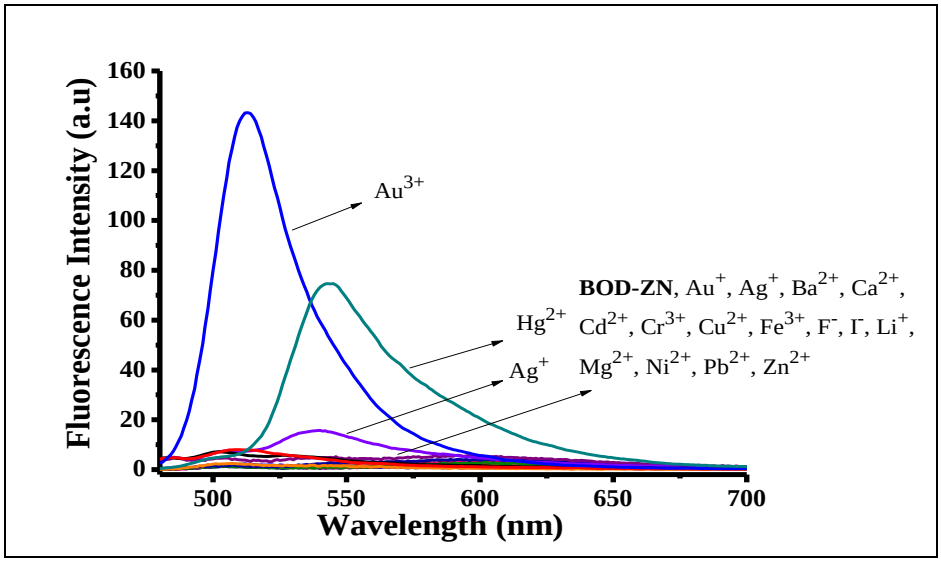

Figure 3.5. Fluorescence intensities of BOD-ZN (10 μM) in 0.1 M phosphate buffer/EtOH (pH = 7.0, v/v, 1:4) in the presence of 20.0 equiv. (200 μM) of the cations interests: BOD-ZN only , Au^{+} , Ba^{2+}, Ca^{2+}, Cd^{2+}, Cr^{3+}, Cu^{2+}, Fe^{3+}, F^{-}, I^{-}, Li^{+}, Mg^{2+}, Ni^{2+}, Pb^{2+}, Zn^{2+}

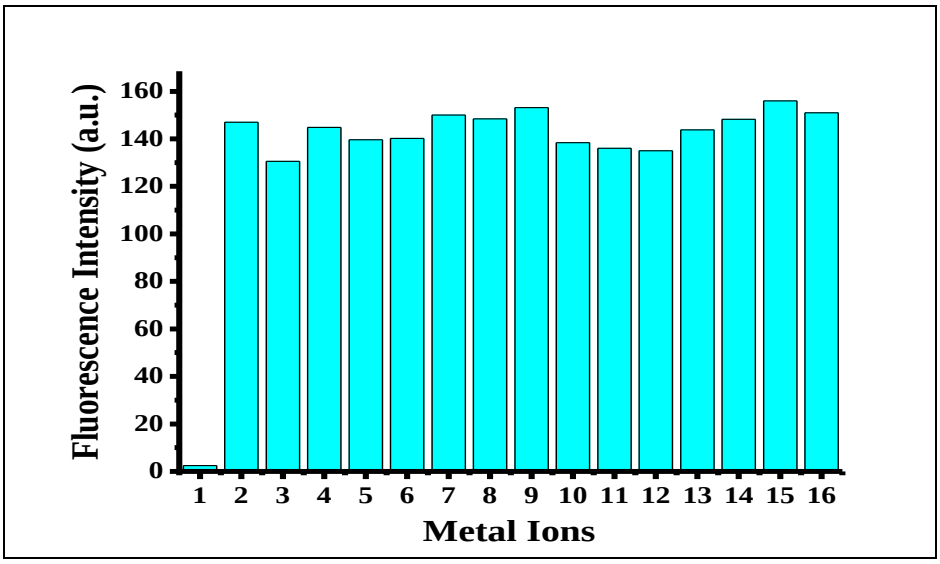

Figure 3.6. Fluorescence intensities of BOD-ZN (10 μM) in 0.1 M phosphate buffer/EtOH (pH = 7.0, v/v, 1:4) in the presence of 10.0 equiv. of Au^{3+} and 20.0 equiv. (200 μM) of the cations interest: 1, BOD-ZN only; 2, none; 3, Au^{+} ; 4, Ba^{2+}; 5, Ca^{2+}; 6, Cd^{2+}; 7, Cr^{3+}; 8, Cu^{2+}; 9, Fe^{3+}; 10, K^{+}; 11, Li^{+}; 12, Mg^{2+}; 13, Ni^{2+}; 14, Zn^{2+}; 15, Ag^{+}; 16, F^{-} (λ_{ex} = 460 nm, λ_{em} = 480 nm)

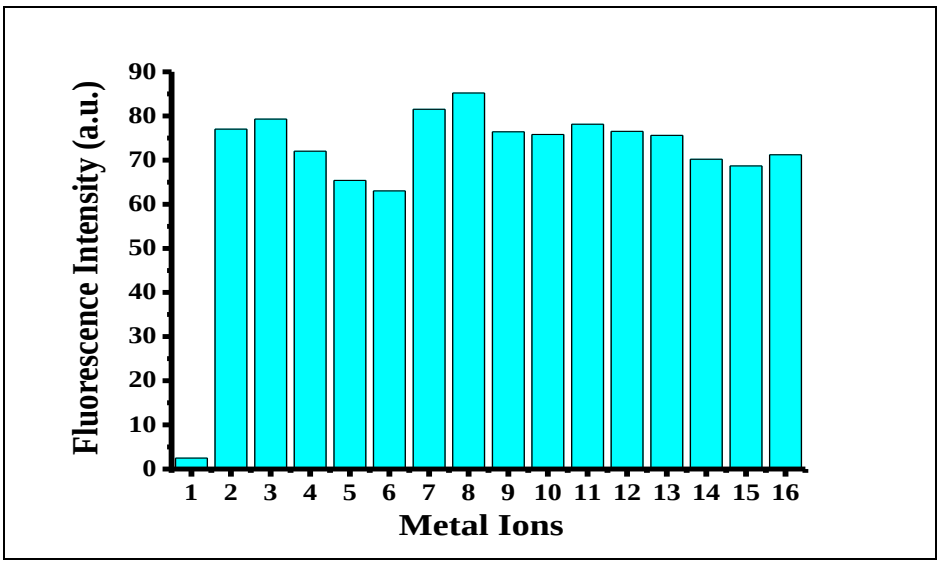

Figure 3.7. Fluorescence intensities of BOD-ZN (10 μM) in 0.1 M phosphate buffer/EtOH (pH = 7.0, v/v, 1:4) in the presence of 10.0 equiv. of Hg^{2+} and 20.0 equiv. (200 μM) of the cations interest**:** 1, BOD-ZN only; 2, none; 3, Au^{+}; 4, Ba^{2+}; 5, Ca^{2+}; 6, Cd^{3+}; 7, Cr^{2+}; 8, Cu^{2+}; 9, Fe^{2+}; 10, I^{-}; 11, Mg^{2+}; 12, Ni^{2+}; 13, Pb^{2+}; 14, Zn^{2+}; 15, Ag^{+}; 16, F^{-} (λ_{ex} = 460 nm, λ_{em} = 480 nm)

As shown in Figure 3.8, the UV/Vis spectrum of free BOD-ZN (Phosphate buffer/Ethanol 1:4, pH 7.0) displayed a maximum absorption band at 533 nm, which belongs to the BODIPY chromophore. In the presence of Au(III) ion, the absorption band shifted to 502 nm. The fluorescence spectrum of BOD-ZN collected upon

excitation at 460 nm exhibited a very weak emission band at 601 nm (Figure 3.9). Reasonably, BOD-ZN was nearly non-emissive, since the molecular structure of the probe bears a C=N functionality that diminishes the emission of the BODIPY core caused by a non-radiative deactivation process involving the rapid isomerization of the C=N group. The addition of Au^{3+} (10 equiv.) to BOD-ZN caused a new emission band to appear at 512 nm that was assigned to the formation of a new BODIPY derivative (Figure 3.10). The appearance of this new band was accompanied with a distinct change in the solution's emission colour; the red-emitting probe solution became distinctly green, that it was clearly visible to the naked eye. The compound displaying such green emission was isolated and further characterized as BOD-AL, the hydrolysis product of BOD-ZN (Figure 3.11). Evidently, the recognition of Au^{3+} was based on an Au^{3+}-mediated hydrolysis reaction that resulted in the formation of a highly emissive BODIPY derivative (BOD-AL).

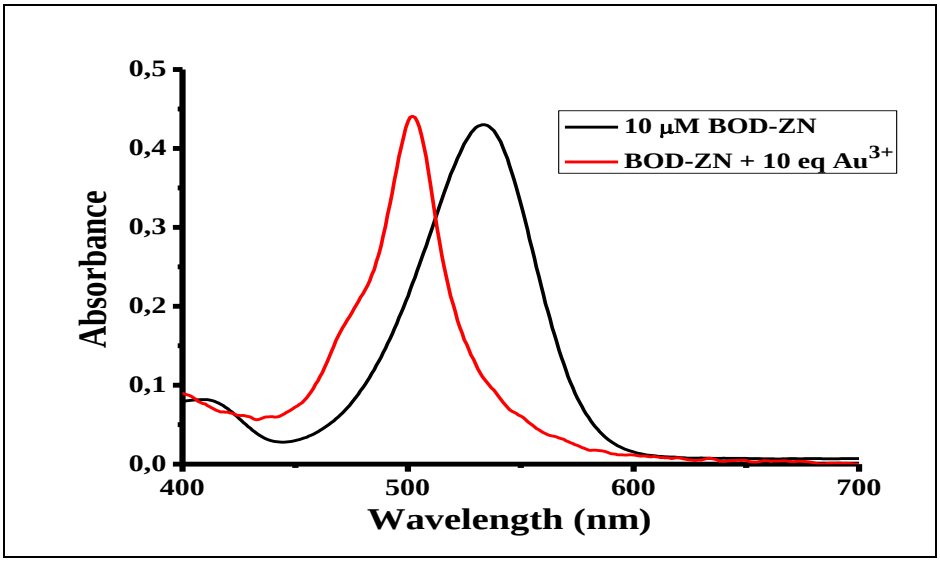

Figure 3.8. Absorbance spectra of BOD-ZN (10 μM) in the presence of 10.0 equiv. (100 μM) of $AuCl_3$ measured in 0.1 M phosphate buffer/EtOH (pH = 7.0, v/v, 1:4) (λ_{ex} = 460 nm, λ_{em} = 480 nm)

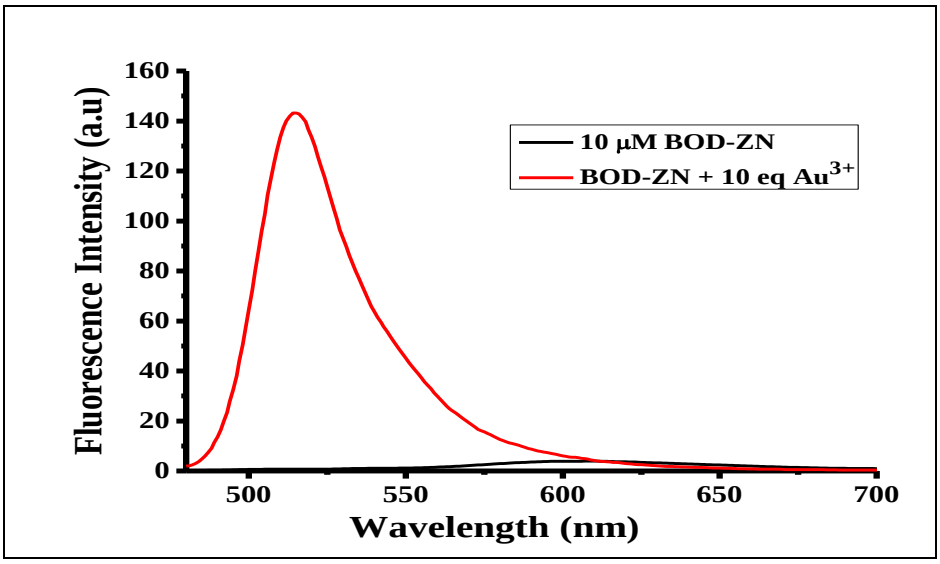

Figure 3.9. Fluorescence spectra of BOD-ZN (10 μM) in the presence of 10.0 equiv. (100 μM) of $AuCl_3$ measured in 0.1 M phosphate buffer/EtOH (pH = 7.0, v/v, 1:4) (λ_{ex} = 460 nm, λ_{em} = 480 nm)

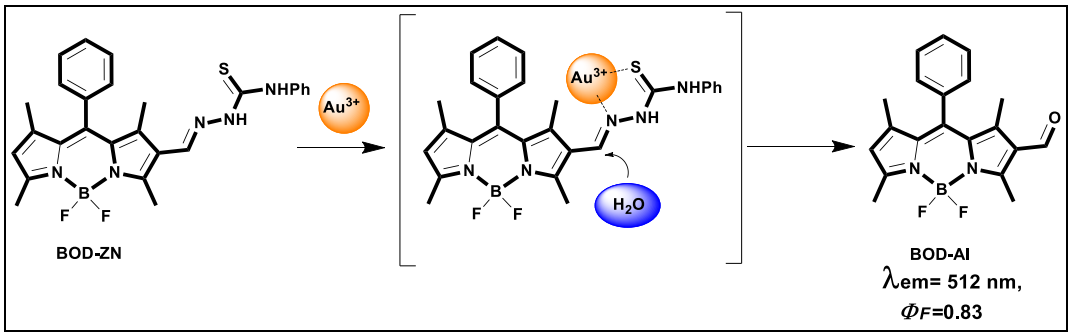

Figure 3.10. Hydrolysis mechanism of BOD-ZN in the presence of Au^{3+}

Figure 3.11. a) Day light photograph image of BOD-ZN + Au(III) (left), BOD-ZN (right), (b) fluoresccence image of BOD-ZN + Au(III) (left), BOD-ZN (right)

A systematic titration of BOD-ZN with Au^{3+} revealed that emission band intensity increases linearly with the increase in concentration of Au^{3+} in the range of 0.1–100 μM. After the addition of 10 equivalents of Au^{3+} ions, the solution became saturated (Figure 3.12). At the same time, the kinetic study showed that the spectral response toward the addition of Au^{3+} was rapid (<1 min) and that the emission intensity plateaued within 20 min due to the addition of 1, 3 and 5 equiv. of Au^{3+}, which thereby enhanced the intensity by over 200-fold (Figure 3.13).

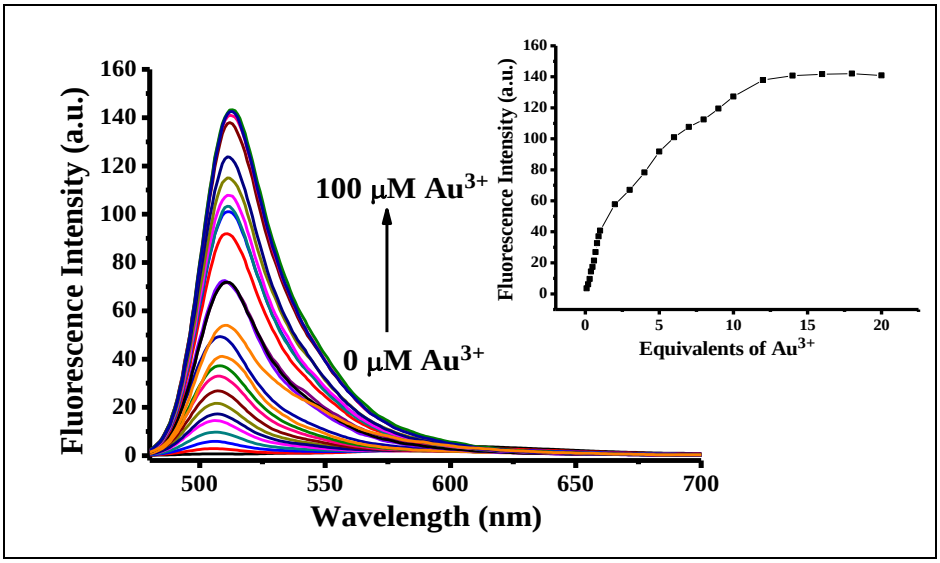

Figure 3.12. Fluorescence spectra of BOD-ZN (10 μM) in 0.1 M phosphate buffer/EtOH (pH = 7.0, v/v, 1:4) in the presence of Au^{3+} (mole equivalents = 0.01-10.0) (0.1-100 μM) (λ_{ex} = 460 nm, λ_{em} = 480 nm) Inset: Fluorescence intensity changes of BOD-ZN vs. equivalents of Au^{3+}

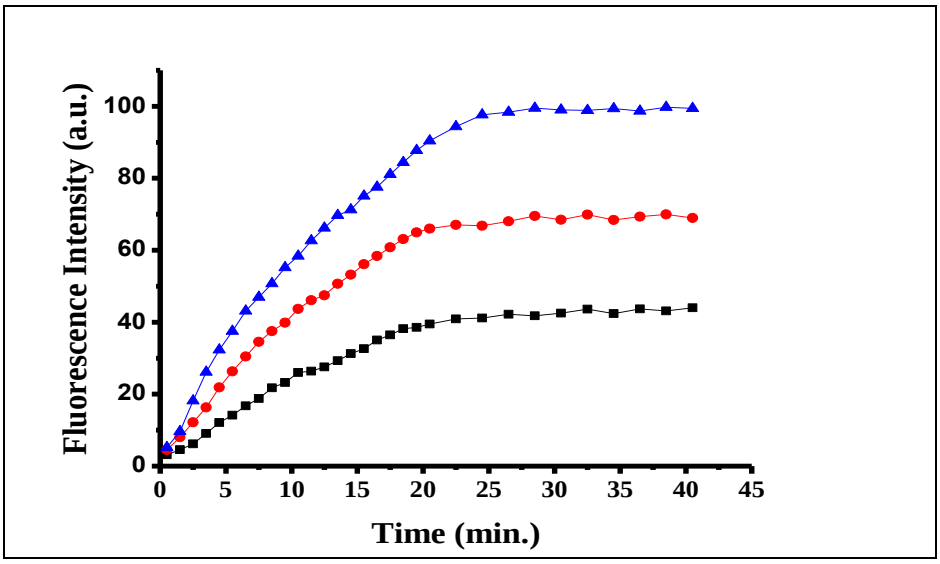

Figure 3.13. Time-dependent fluorescence change of BOD-ZN (10 μM) in the presence of 1.0 (■), 3.0 (●) and 5.0 (▲) equiv. (10, 30 and 50 μM) of $AuCl_3$ measured in 0.1 M phosphate buffer/EtOH (pH = 7.0, v/v, 1:4) (λ_{ex} = 460 nm, λ_{em} = 480 nm)

Moreover, the minimum amount of Au^{3+} detectable was evaluated based on the fluorescence titration (Emrullahoğlu et al., 2013). To determine the S/N ratio, the emission intensity of BOD-ZN (10 μM) without Au^{3+} was measured 10 times and the standard deviation of blank measurements was determined. Under the present conditions, a good linear relationship between the fluorescence intensity and Au^{3+} concentration could be obtained in the 0.1-1.0 μM (R = 0.9915) (Figure 3.14). The detection limit is then calculated using the equation: detection limit = 3σbi/m, where σbi is the standard deviation of blank measurements; m is the slope between intensity versus sample concentration. The detection limit was determined to be 128 nM at S/N = 3.

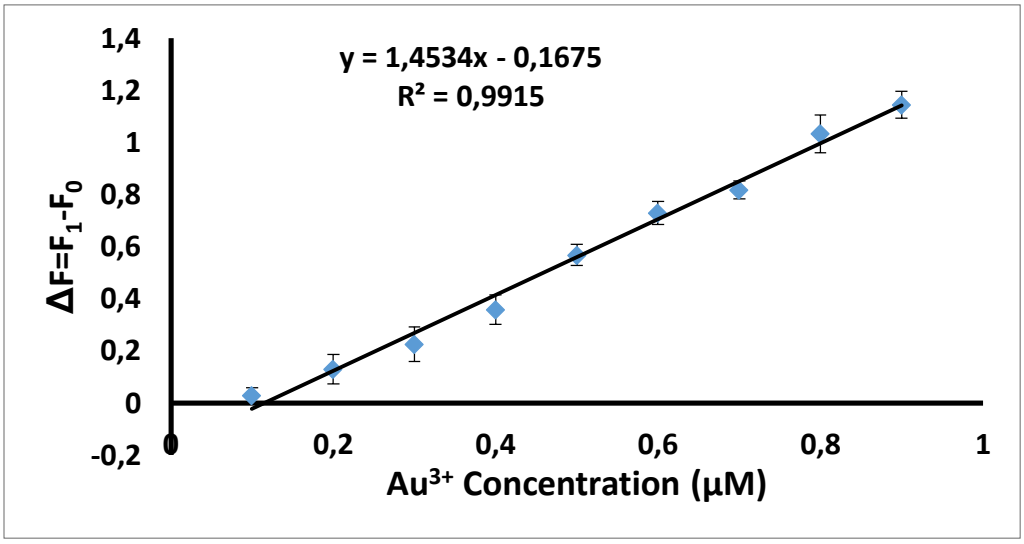

Figure 3.14. Fluorescence changes of BOD-ZN (10 μM) in 0.1 M phosphate buffer/EtOH (pH = 7.0, v/v, 1:4) upon the addition of Au^{3+} (0.01 to 0.1 equiv.) (0.1-1 μM)

The detection of Hg^{2+} was recognized with a different absorption and emission output. While free BOD-ZN displayed a maximum absorption band at 533 nm, in the presence of Hg(II) ion, this absorption band shifted to 520 nm (Figure 3.15). Meanwhile, in the fluorescence spectrum of BOD-ZN, a new emission band appeared at 542 nm with the rapid addition of Hg^{2+} ion as shown in Figure 3.16.

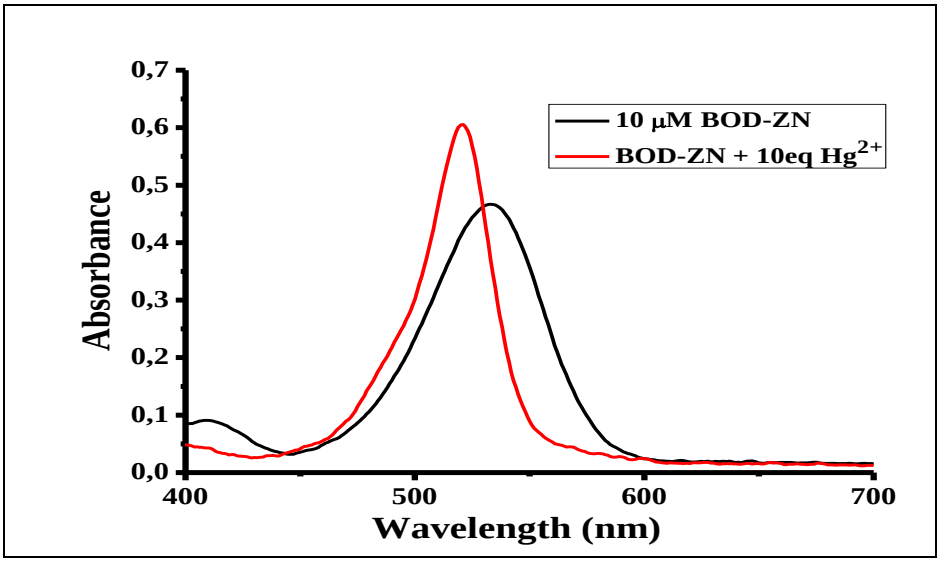

Figure 3.15. Absorbance spectra of **BOD-ZN** (10 μM) in the presence of 10.0 equiv. (100 μM) of $HgCl_2$ measured in 0.1 M phosphate buffer/EtOH (pH = 7.0, v/v, 1:4)

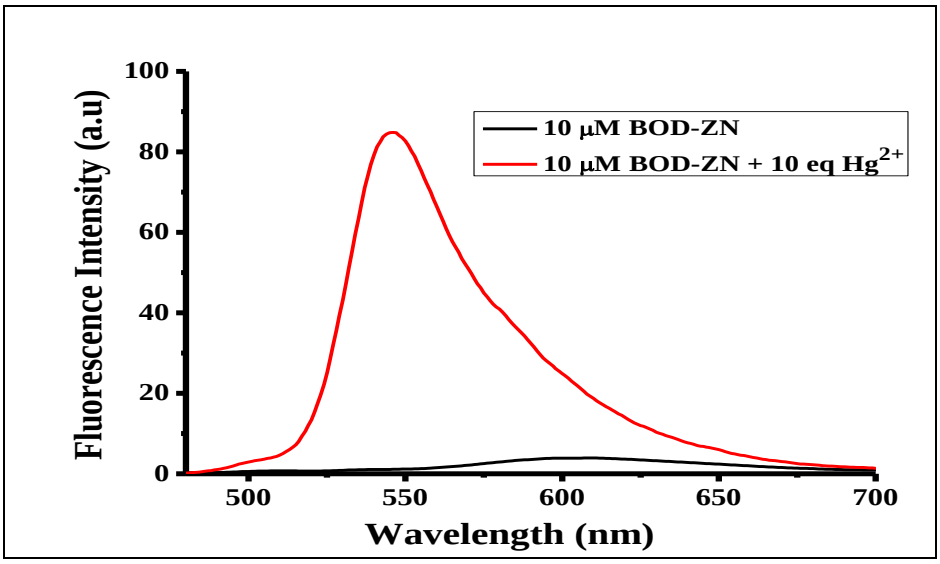

Figure 3.16. Fluorescence spectra of **BOD-ZN** (10 μM) in the presence of 10.0 equiv. (100 μM) of $HgCl_2$ measured in 0.1 M phosphate buffer/EtOH (pH = 7.0, v/v, 1:4)

Given the addition of Hg^{2+}, the weakly emissive probe solution (<5 sec) turned immediately and profoundly yellow, possibly due to the blockage of the free rotation around the axis, which prevents the isomerization of the C=N bond, thus enhancing the fluorescence emission (Figure 3.17).

Figure 3.17. a) Day light photograph image of BOD-ZN + Hg(II) (left), BOD-ZN (right), (b) fluoresccence image of BOD-ZN + Hg(II) (left), BOD-ZN (right)

According to the titration experiment of BOD-ZN with Hg^{2+} ion, emission band intensity increased linearly with the increase in concentration of Hg^{2+} in the range of 0.1–100 μM. After the addition of 10 equivalents of Hg^{2+} ions, the solution became saturated (Figure 3.18). Meanwhile, kinetic study showed that the response of the probe

toward Hg^{2+} ion was so rapid (<5 sec) and that enhanced emission intensity at 542 nm started to decrease 10 minutes later than the addition of the metal ion and a new emission band at 512 nm appeared (Figure 3.19).

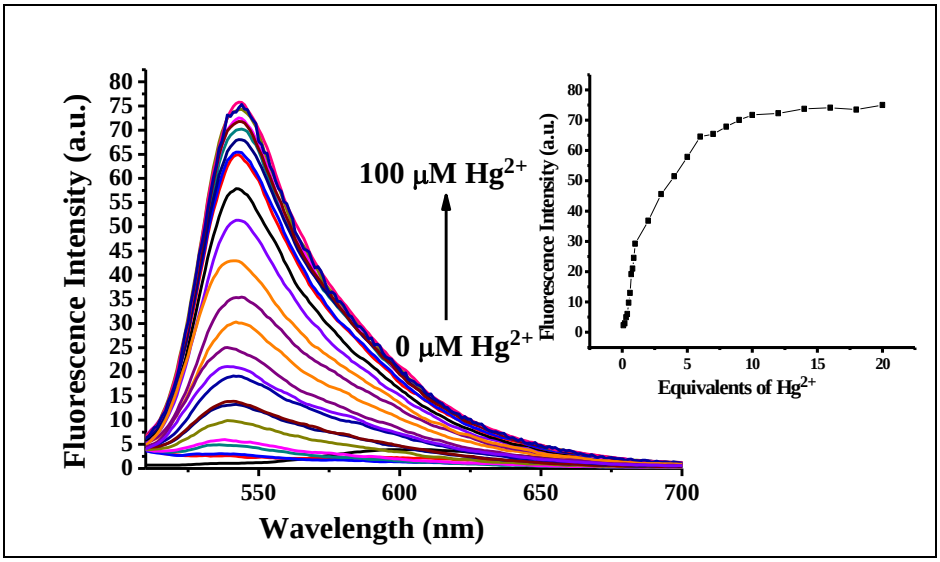

Figure 3.18. Fluorescence spectra of BOD-ZN (10 μM) in 0.1 M phosphate buffer/EtOH (pH = 7.0, v/v, 1:4) in the presence of Hg^{2+} (mole equivalents = 0.01-10.0) (0.1-100 μM) (λ_{ex} = 460 nm, λ_{em} = 480 nm) Inset: Fluorescence intensity changes of BOD-ZN vs. equivalents of Hg^{2+}

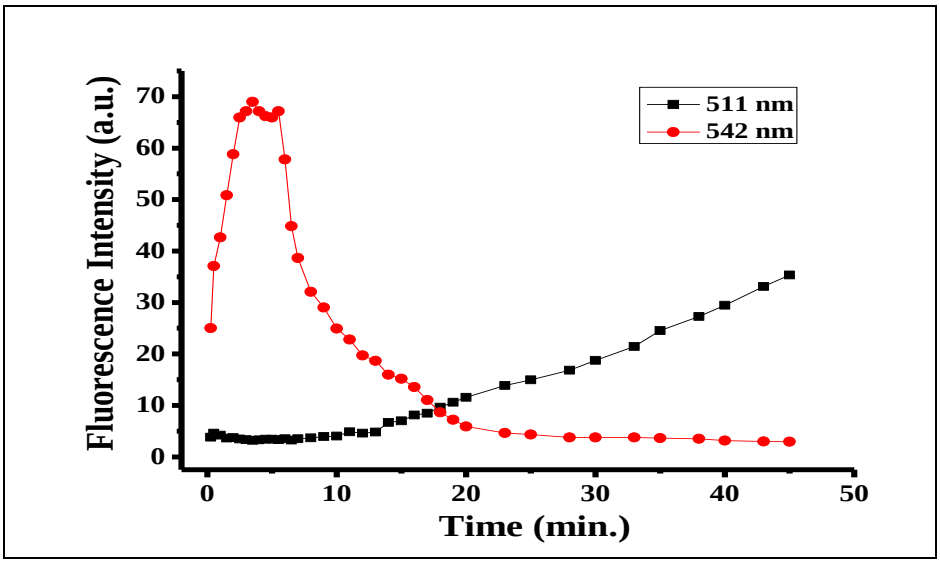

Figure 3.19. Time-dependent fluorescence change of BOD-ZN (10 μM) measured in 0.1 M Phosphate Buffer/EtOH (pH = 7.0, v/v, 1:4) in the presence of 10 equiv. (100 μM) of $HgCl_2$ (λ_{ex} = 460 nm, λ_{em} = 480 nm)

In Figure 3.19, it is clearly seen that the emission band at 542 nm almost disappeared in process of time. The same tendency was observed while investigating the selectivity of BOD-ZN in the presence of both Hg^{2+} and Au^{3+} ions. In this part of the study, the probe first gave an emission band at 542 nm indicating the presence of Hg(II) ion. However, this band nearly disappeared within 30 minutes and by the time of progress the emission band at 512 nm started to increase (Figure 3.20). Though, it is not for certain whether this band indicates the Au^{3+}-mediated hydrolysis reaction product or degradation of Hg-complex as it was observed in kinetic study.

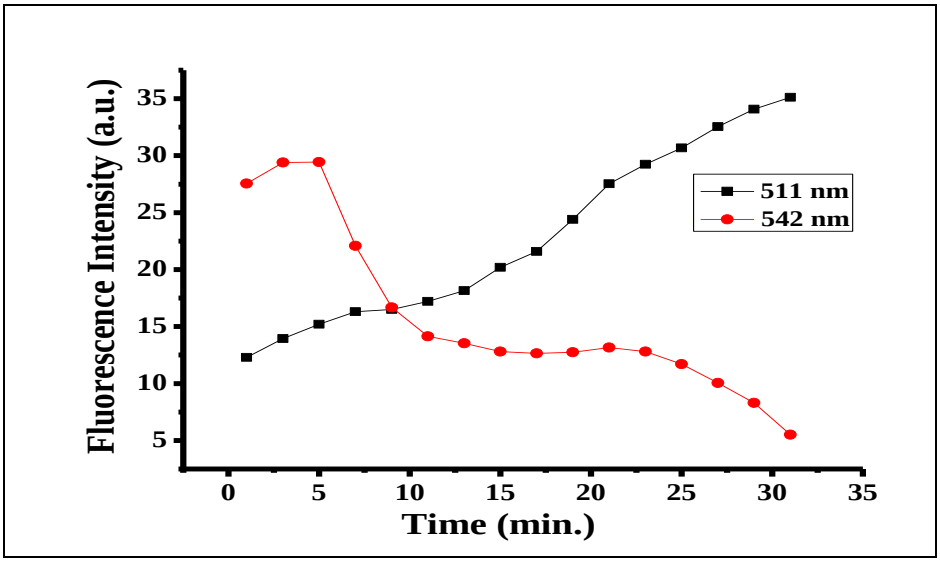

Figure 3.20. Selectivity of BOD-ZN (10 μM) in the presence of both Hg^{2+} and Au^{3+} (10 equiv., 100 μM) in 0.1 M phosphate buffer/EtOH (pH 7.0, v/v, 1:4) (λ_{ex} = 460 nm, λ_{em} = 480 nm)

The minimum amount of Hg^{2+} detectable was determined based on fluorescence titration as it was done before for Au(III) ion. Under the present conditions, a good linear relationship between the fluorescence intensity and Hg^{2+} concentration could be obtained in the 0.1-1.0 μM (R = 0.9931) (Figure 3.21). The detection limit was measured to be 160 nM at S/N = 3.

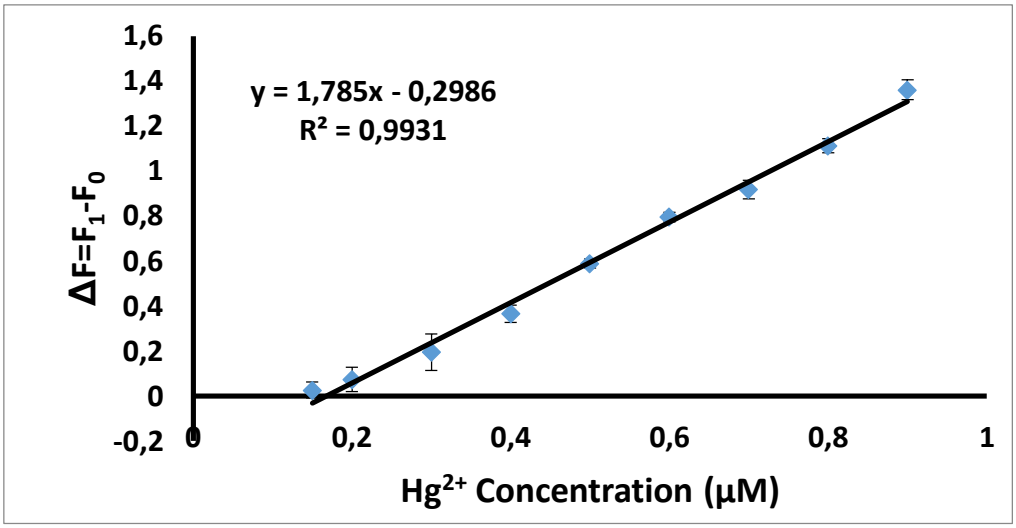

Figure 3.21. Fluorescence changes of BOD-ZN (10 μM) in 0.1 M phosphate buffer/EtOH (pH = 7.0, v/v, 1:4) upon addition of Hg^{2+} (0.01 to 0.1 equiv.) (0.1-1 μM)

To detect whether the sensing process of Hg^{2+} ion is reversible or not, excess amounts of various compounds such as KCN, tetrabutylammonium cyanide, Na_2S and tetrabutylammonium hydroxide were tested. The reversibility of the binding event between BOD-ZN and Hg^{2+} was confirmed by the addition of Na_2S to the solution pretreated with Hg^{2+}, which decreased the emission intensity sharply. In the presence of 10 equiv. of Na_2S, S^{2-} ion due to its strong affinity for Hg^{2+} ions formed complex with it resulting in decomplexation of receptor-Hg^{2+} complex. The regeneration of fluorescence was again made possible by introducing Hg^{2+} ions into the solution, and the off-on switching ability of the system with Hg^{2+} proved the reversibility of the process (Figure 3.23).

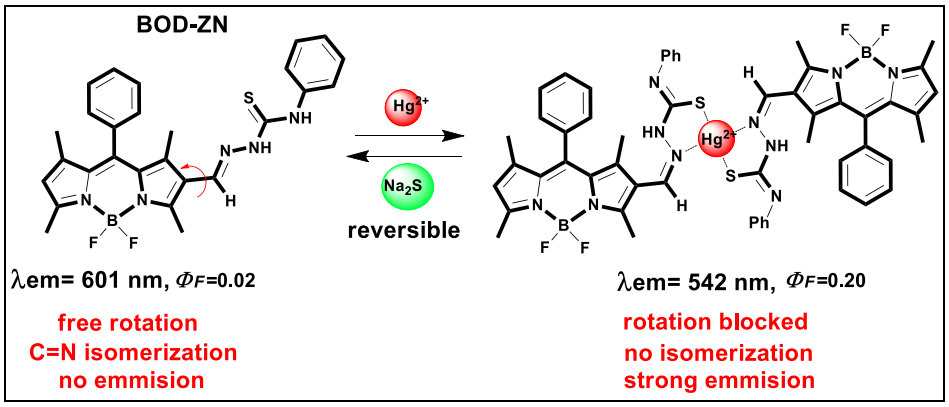

Figure 3.22. Reversible binding of Hg^{2+} to BOD-ZN

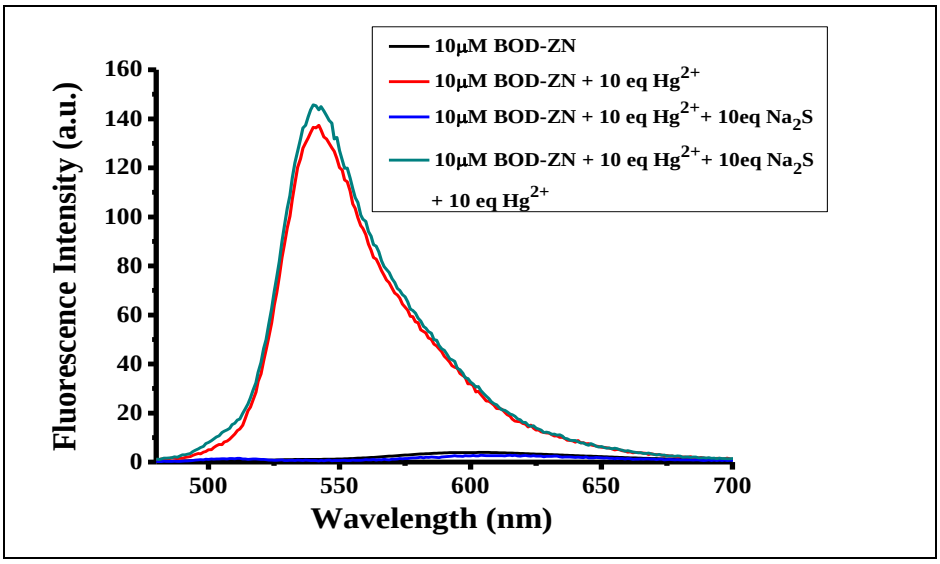

Figure 3.23. Fluorescence intensity changes of BOD-ZN (10 μM) in EtOH at pH = 7.0 at λ_{max} =542 nm after the addition of 10 equiv. Hg^{2+}, 10 equiv. Hg^{2+} + 10 equiv. Na_2S, 10 equiv. Hg^{2+} + 10 equiv. Na_2S + 10 equiv. Hg^{2+}, respectively. (λ_{ex} = 460 nm, λ_{em} = 480 nm)

The stoichiometry of the sensing event was established by the following Benesi-Hildebrand method and, accordingly, the related binding constant was determined to be 4.2 x 10^4 M^{-2} with a 1:2 binding stoichiometry (Benesi et al., 1949). The associacion constant of [Hg^{2+}] was determined by using fluorescence titration data with the help of the following equation;

$$\ln[(F - F_0) / (F_{max} - F_0)] = n \ln[Hg^{2+}] + n \ln(K_{asscn}) \quad \text{.....(1)}$$

where n is the number of mercury ions associated with each molecule of BOD-ZN, K_{assoc} is the association constant, F_0 is the fluorescence of the free probe, F_{max} is the fluorescence intensity at saturation point, and F is the fluorescence of the probe obtained with Hg^{2+} addition (Figure 3.24). With HRMS analysis, the binding of Hg^{2+} ions to BOD-ZN was also confirmed. HRMS data of the solution (Hg^{2+}/BOD-ZN**)** indicated the formation of an Hg^{2+} ion complex, (*m/z* = 1204.36841 found; 1204.36354 calc.), with a binding stoichiometry of 1:2. Given all of the above, the structure of the binding complex is most likely to be represented as shown in Figure 3.22.

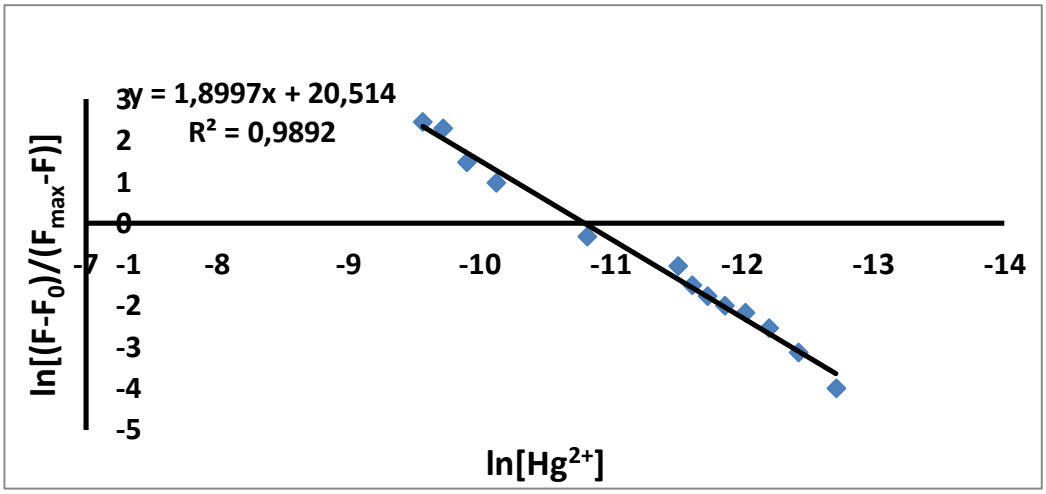

Figure 3.24. Plot of $\ln[(F-F_0)/(F_{max}-F)]$ against $\ln[Hg^{2+}]$; the stoichimetry of BOD-ZN Hg^{2+} association, obtained directly from the slope, is 1.9 ≅ 2. Following equation 1, the intercept represented an association constant of BOD-ZN which is equal to 4.2 x 10^4 M^{-2} (in 0.1 M potassium phosphate buffer, pH 7.0/EtOH (v/v, 1:4) (λ_{ex}: 460 nm, λ_{em} = 480 nm at 25 ^oC).

At the same time, the binding process of Hg^{2+} to BOD-ZN could be clearly followed by the aid of ^{1}H-NMR spectroscopy. During Hg^{2+} incubation which lasts 5 min, pronounced differences in the ^{1}H-NMR spectrum of BOD-ZN were observed. For one, the resonance of the H_a proton signal at 8.01 ppm belonging to the hydrogen atom of the aldimine shifted to a higher frequency, while the resonance of the methyl protons (H_b and H_c) in close proximity to the recognition motif shifted to a lower frequency. Furthermore, a reorganization of the phenyl ring proton signals strongly suggests a structural modification in the phenyl thiourea motif (Figure 3.25).

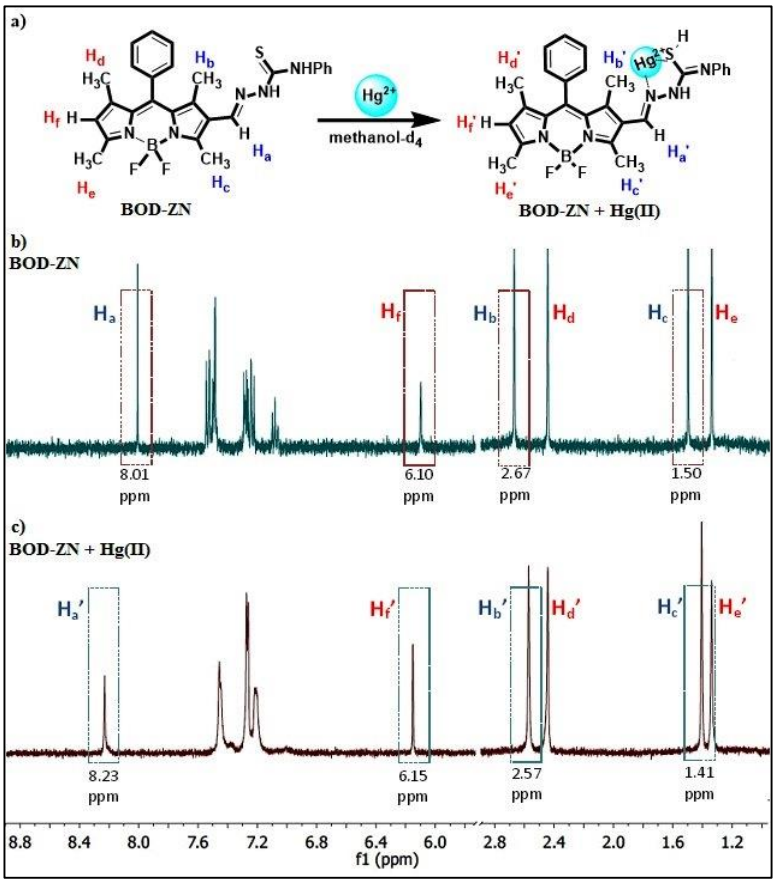

Figure 3.25. a) Proposed coordination mechanism of Hg^{2+} to BOD-ZN. b) ^{1}H-NMR of BOD-ZN in methanol-d_4. c) ^{1}H-NMR of BOD-ZN + Hg^{2+} (1 equiv.) in methanol-d_4.

As the last work of the study, the capacity of BOD-ZN for imaging Hg^{2+} and Au^{3+} ions in living cells was investigated. As Figure 3.26a and 3.26a' show, the images of human lung adenocarcinoma (A549) cells incubated with BOD-ZN did not display any fluorescence until the addition of the metal species. However, upon incubation with Au^{3+} or Hg^{2+}, the cells started to display a distinct fluorescence emission consistent with the results obtained in the solution. Based on the nucleus staining experiment using DAPI as the staining dye, it was concluded that the probe passes through the cell membrane and detects both metal species from within the cell. This preliminary cell imaging study suggested that BOD-ZN can be used efficiently for *in vitro* imaging of Au^{3+} and Hg^{2+} species in living cells.

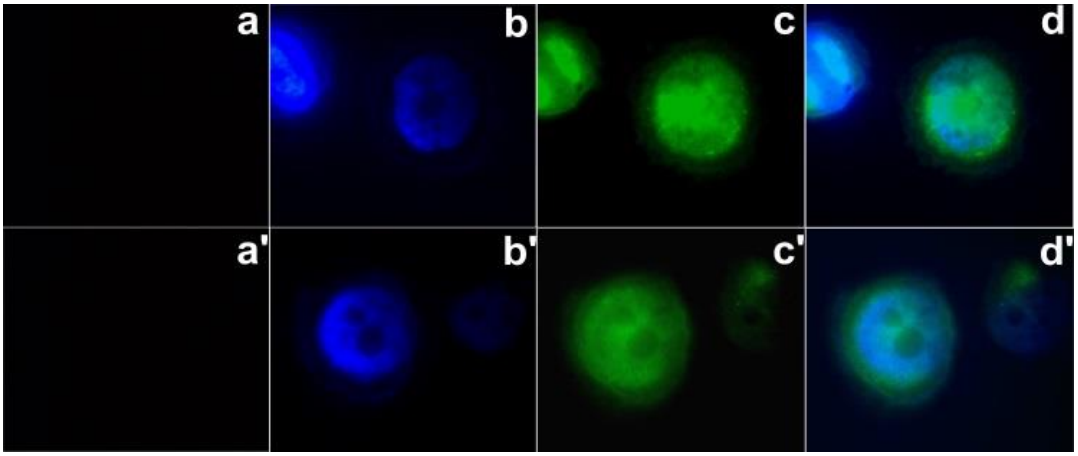

Figure 3.26. Fluorescence images of Human Lung Adenocarcinoma cells (A549). a,a') Fluorescence image of A549 cells treated with BOD-ZN (10 μM) only; b, b') Fluorescence image of cells treated with DAPI (control); c, c') Fluorescence image of cells treated with BOD-ZN (10 μM) and Au^{3+} (10 μM) or Hg^{2+} (10 μM) (λ_{ex} = 460 nm); d, d') merged images of frames b-c or b'-c'.

CHAPTER 4

CONCLUSION

In summary, a new type of BODIPY-based turn-on fluorescent molecular sensor that can differentiate Hg^{2+} and Au^{3+} ions was developed. The differential detection of Hg^{2+} and Au^{3+} was recognized in two distinct fluorescence changes: one resulting from a reversible Hg^{2+}/sensor complex formation, the other an irreversible Au^{3+}-mediated hydrolysis reaction. Before the addition of any metal species, BOD-ZN was nearly non-emissive since the molecular structure of the probe had a C=N functionality that diminished the emission of the BODIPY core caused by a non-radiative deactivation process involving the rapid isomerization of the C=N group. The probe showed no spectral response to any other metal species except for Au^{3+} and Hg^{2+} ions.

The hydrolysis reaction product of BOD-ZN was isolated and characterized as a highly emissive BODIPY derivative, BOD-AL. While the detection of Au^{3+} ions required an irreversible reaction, detecting Hg^{2+} ions proceeded reversibly by the addition of Na_2S to the solution pretreated with Hg^{2+}. The stoichiometry of the sensing event was established by following the Benesi-Hildebrand method and, accordingly, the related binding constant was determined to be 4.2×10^4 M^{-2}. Also, HRMS analysis confirmed the formation of a Hg^{2+} ion complex (*m/z* = 1204.36841 found; 1204.36354 calc.) with a binding stoichiometry of 1:2. The detection limits of both Au^{3+} and Hg^{2+} ions were determined to be 128 nM and 160 nM, respectively.

Cell imaging capacity of the developed molecular sensor was studied in human lung adenocarcinoma (A549) cells. No fluorescence was observed in the cell images before the addition of the metal species; however, upon incubation with Au^{3+} or Hg^{2+}, the cells started to emit a fluorescence emission and it was concluded that the probe was able to pass through cell membrane and detected both metal species in cell lines.

REFERENCES

Onyido, I.; Norris, A. R.; Buncel, E. Biomolecule-Mercury Interactions: Modalities of DNA Base-Mercury Binding Mechanisms. Remediation Strategies. Chem. Rev. 2004, 104, 5911-5929.

Yang, Y.-K; Lee, S.; Tae, J. A. Gold(III) Ion Selective Fluorescent Probe and Its Application to Bioimagings. Org. Lett. 2009, 11, 5610-5613.

Do, J. H.; Kim, H. N.; Yoon, J.; Kim, J. S.; Kim, H.-J. A Rationally Designed Fluorescence Turn-on Probe For the Gold(III) Ion. Org. Lett. 2010, 12, 932-934.

Emrullahoglu, M.; Karakus, E.; Ucuncu, M. A Rhodamine Based Turn-on Chemodosimeter For Monitoring Gold Ions in Synthetic Samples and Living Cells. Analyst, 2013, 138, 3638-3641.

Quang, D. T.; Kim, J. S. Fluoro- and Chromogenic Chemodosimeters For Heavy Metal Ion Detection in Solution and Biospecimens. Chem. Rev. 2010, 110, 6280-6301.

Chae, M.-Y.; Czarnik, A. W. Fluorometric Chemodosimetry. Mercury(II) and Silver(I) Indication in Water via Enhanced Fluorescence Signaling. J. Am. Chem. Soc. 1992, 114, 9704-9705.

Treibs, A.; Kreuzer, F. Difluorboryl-Komplexe von Di- and Tripyrrylmethenen. Justus Liebigs Ann. Chem. 1968, 718, 208-223.

Boens, N.; Leen, V.; Dehaen, W. Fluorescent Indicators Based on Bodipy. Chem. Soc. Rev. 2012, 41, 1130-1172.

Wood, T.; Thompson, A. Advances in the Chemistry of Dypyrrins and Their Complexes. Chem. Rev. 2007, 107, 1831-1861.

Littler, B. J.; Miller, M. A.; Hung, C.-H.; Wagner, R. W.; O'Shea, D. F.; Boyle, P. D.; Lindsey, J. S. Refined Synthesis of 5-Substituted Dipyrromethanes. J. Org. Chem. 1999, 64, 1391-1396.

Li, Z.; Mintzer, E.; Bittman, R. First Synthesis of Free Cholesterol-BODIPY Conjugates. J. Org. Chem. 2006, 71, 1718-1721.

Shah, M.; Thangaraj, K.; Soong, M.-L.; Wolford, L. T.; Boyer, J. H.; Politzer, I. R.; Pavlopoulos, T. G. Pyrromethenes-BF_2 Complexes As Laser Dyes. Heteroat. Chem. 1990, 1, 389.

Yakubovskyi, V. P.; Shandura, M. P.; Kovtun, Y. P. Boradipyrromethenecyanines. Eur. J. Org. Chem. 2009, 2009, 3237-3243.

Wu, L.; Burgess, K. A New Synthesis of Symmetric Boraindacene (BODIPY) Dyes. Chem. Commun. 2008, 4933-4935.

Schmitt, A.; Hinkeldey, B.; Wild, M. Synthesis of the Core Compound of the BODIPY Dye Class: 4,4'- Difluoro-4-bora-(3a, 4a)-diaza-s-indacene. J. Fluoresc. 2009, 19, 755-758.

Leen, V.; Auweraer, M. V.; Boens, N.; Dehaen, W. Vicarious Nucleophilic Substitution of α-Hydrogen of BODIPY and Its Extension to Direct Ethenylation. Org. Lett. 2011, 13, 1470-1473.

Gabe, Y.; Urano, Y.; Kikuchi, K.; Kojima, H.; Nagano, T. Highly Sensitive Fluorescence Probes for Nitric Oxide Based on Boron Dipyrromethene Chromophore- Rational Design of Potentially Useful Bioimaging Fluorescence Probe. J. Am. Chem. Soc. 2004, 126, 3357-3367.

Verbelen, B.; Leen, V.; Wang, L.; Boens, N.; Dehaen, W. Direct Palladium Catalyzed C-H Arylation of BODIPY Dyes at the 3- and 3,5- Positions. Chem. Commun. 2012, 48, 9129-9131.

Huang, L.; Yu, X.; Wu, W.; Zhao, J. Styryl Bodipy-C_{60} Dyads As Efficient Heavy-Atom-Free Organic Triplet Photosensitizers. Org. Lett. 2012, 14, 2594-2597.

Leen, V.; Yuan, P.; Wang, L.; Boens, N.; Dehaen, W. Synthesis of Meso-Halogenated BODIPYs and Access to Meso-Substituted Analogues. Org. Lett. 2012, 14, 6150-6153.

Rohand, T.; Baruah, M.; Qin, W.; Boens, N.; Dehaen, W. Functionalisation of Fluorescent BODIPY Dyes by Nucleophilic Substitution. Chem. Commun. 2006, 266-268.

Ozlem, S.; Akkaya, E. U. Thinking Outside the Silicon Box: Molecular and Logic As an Additional Layer of Selectivity in Singlet Oxygen Generation for Photodynamic Therapy. J. Am. Chem. Soc. 2009, 131, 48-49.

Barin, G.; Yilmaz, M. D.; Akkaya, E. U. Boradiazaindacene (Bodipy)-Based Building Blocks For the Construction of Energy Transfer Cassettes. Tetrahedron Lett. 2009, 50, 1738-1740.

Bozdemir, O. A.; Guliyev, R.; Buyukcakir, D.; Selcuk, S.; Kolemen, S.; Gulseren, G.; Nalbantoglu, T.; Boyaci, H.; Akkaya, E. U. Selective Manipulation of ICT and PET Processes in Styryl-Bodipy Derivatives: Applications in Molecular Logic and Fluorescence Sensing of Metal Ions. J. Am. Chem. Soc. 2010, 132, 8029-8036.

Bozdemir, O. A.; Sozmen, F.; Buyukcakir, D.; Guliyev, R.; Cakmak, Y.; Akkaya, E. U. Reaction-Based Sensing of Fluoride Ions Using Built-in Triggers For Intramolecular Charge Transfer and Photoinduced Electron Transfer. Org. Lett. 2010, 12, 1400-1403.

Yang, Y.-K; Lee, S.; Tae, J. A Gold(III) Ion-Selective Fluorescent Probe and Its Application to Bioimagings. Org. Lett. 2009, 11, 5610-5613.

a) Cho, D.-G.; Sessler, J. L. Modern Reaction-Based Indicator Systems. Chem. Soc. Rev. 2009, 38, 1647-1662. b) Dujols, V.; Ford, F.; Czarnik, A. W. A Long-Wavelength Fluorescent Chemodosimeter Selective For Cu(II) Ion in Water. J. Am. Chem. Soc. 1997, 119, 7386-7387.

Jou, M. N.; Chen, X.; Swamy, K. M. K.; Kim, H. N.; Kim, H.-J.; Lee, S.; Yoon, J. Highly Selective Fluorescent Probe For Au^{3+} Based on Cyclization of Propargylamide. Chem. Commun. 2009, 7218-7220.

Egorova, O. A.; Seo, H.; Chatterjee, A.; Ahn, K. H. Reaction-Based Fluorescent Sensing of Au(I)/Au(III) Species: Mechanistic Implications on Vinylgold Intermediates. Org. Lett. 2010, 12, 401-403.

Do, J. H.; Kim, H. N.; Yoon, J.; Kim, J. S.; Kim, H.-J. A Rationally Designed Fluorescence Turn-on Probe For the Gold(III) Ion. Org. Lett. 2010, 12, 932-934.

Dong, M.; Wang, Y.-W.; Peng, Y. Highly Selective Ratiometric Fluorescent Sensing For Hg^{2+} and Au^{3+}, Respectively, in Aqueous Solution. Org. Lett. 2010, 12, 5310-5313.

Wang, J.-B.; Wu, Q.-Q.; Min, Y.-Z.; Liu, Y.-Z.; Song, Q.-H. A novel Fluorescent Probe For Au(III)/Au(I) Ions Based on an Intramolecular Hydroamination of a BODIPY Derivative and Its Application to Bioimaging. Chem. Commun. 2012, 48, 744-746.

Patil, N. T.; Shinde, V. S.; Thakare, M. S.; Kumar, P. H.; Pangal, P. T.; Barui, A. Y. Patra, C. R. Exploiting the Higher Alkynophilicity of Au Species: Development of a Highly Selective Fluorescent Probe For Gold Ions. Chem. Commun. 2012, 48, 11229-11231.

Karakus, E.; Ucuncu, M.; Emrullahoglu, M. A Rhodamine/BODIPY-Based Fluorescent Probe For the Differential Detection of Hg(II) and Au(III). Chem. Commun. 2014, 50, 1119-1121.

Fabbrizzi, L.; Lichelli, M.; Pallavicini, P.; Perotti, A.; Sacchi, D. An Anthracene-Based Fluorescent Sensor For Transition Metal Ions. Angew. Chem. Int. Ed. 1994, 33, 1975-1977.

Yang, Y.-K.; Yook, K-J.; Tae, J. A Rhodamine-Based Fluorescent and Colorimetric Chemodosimeter For the Rapid Detection of Hg^{2+} Ions in Aqueous Media. J. Am. Chem. Soc. 2005, 127, 16760-16761.

Wu, J.-S.; Hwang, I.-C.; Kim, K. S.; Kim, J. S. Rhodamine-Based Hg^{2+}-Selective Chemodosimeter in Aqueous Solution: Fluorescent OFF-ON. Org. Lett. 2007, 9, 907-910.

Coskun, A.; Yilmaz, M. D. Akkaya, E. U. Bis(2-pyridyl)-Substituted Boratriazaindacene As an NIR-Emitting Chemosensor For Hg(II). Org. Lett. 2007, 9, 607-609.

Shang, G.-Q.; Gao, X.; Chen, M.-X.; Zheng, H.; Xu, J.-G. A Novel Hg^{2+} Selective Ratiometric Fluorescent Chemodosimeter Based on an Intramolecular FRET Mechanism. J. Fluoresc. 2008, 18, 1187-1192.

Fan, J.; Guo, K.; Peng, X.; Du, J.; Wang, J.; Sun, S.; Li, H. A Hg^{2+} Fluorescent Chemosensor Without Interference From Anions and Hg^{2+}-Imaging in Living Cells. Sens. Actuators, B. 2009, 142, 191-196.

Atilgan, S.; Ozdemir, T.; Akkaya, E. U. Selective Hg(II) Sensing With Improved Stokes Shift By Coupling the Internal Charge Transfer Process to Excitation Energy Transfer. Org. Lett. 2010, 12, 4792-4795.

Kim, H. N.; Nam, S.-W.; Swamy, K. M. K.; Jin, Y.; Chen, X.; Kim, Y.; Kim, S.-J.; Park, S.; Yoon, J. Rhodamine Hydrazone Derivatives As Hg^{2+} Selective Fluorescent and Colorimetric Chemosensors and Their Applications to Bioimaging and Microfluidic System. Analyst, 2011, 136, 1339-1343.

Bera, K.; Das, A. K.; Nag, M.; Basak, S. Development of a Rhodamine-Rhodanine-Based Fluorescent Mercury Sensor and Its Use To Monitor Real-Time Uptake and Distribution of Inorganic Mercury in Live Zebrafish Larvae. Anal. Chem. 2014, 86, 2740-2746.

Cunha, S.; Da Silva, T. L. One-Pot and Catalyst-Free Synthesis of Thiosemicarbazones via Multicomponent Coupling Reactions. 2009, 50, 2090-2093.

Wu, W.; Guo, H.; Wu, W.; Ji, S.; Zhao, J. Organic Triplet Sensitizer Library Derived From a Single Chromophore (BODIPY) With Long-Lived Triplet Excited State For Triplet-Triplet-Annihilation Based Upconversion. J. Org. Chem. 2011, 76, 7056-7064.

Liu, J.-Y.; Yeung, H.-S.; Xu, W.; Li, X.; Ng, D. K. P. Highly Efficient Energy Transfer in Subphtalocyanine-BODIPY Conjugates. Org. Lett. 2008, 10, 5421-5424.

Isik, M.; Ozdemir, T.; Turan, I. S.; Kolemen, S.; Akkaya, E. U. Chromogenic and Fluorogenic Sensing of Biological Thiols in Aqueous Solutions Using Bodipy Based Reagents. Org. Lett. 2013, 15, 216-219.

APPENDIX A

^{1}H-NMR AND ^{13}C-NMR SPECTRA OF COMPOUNDS

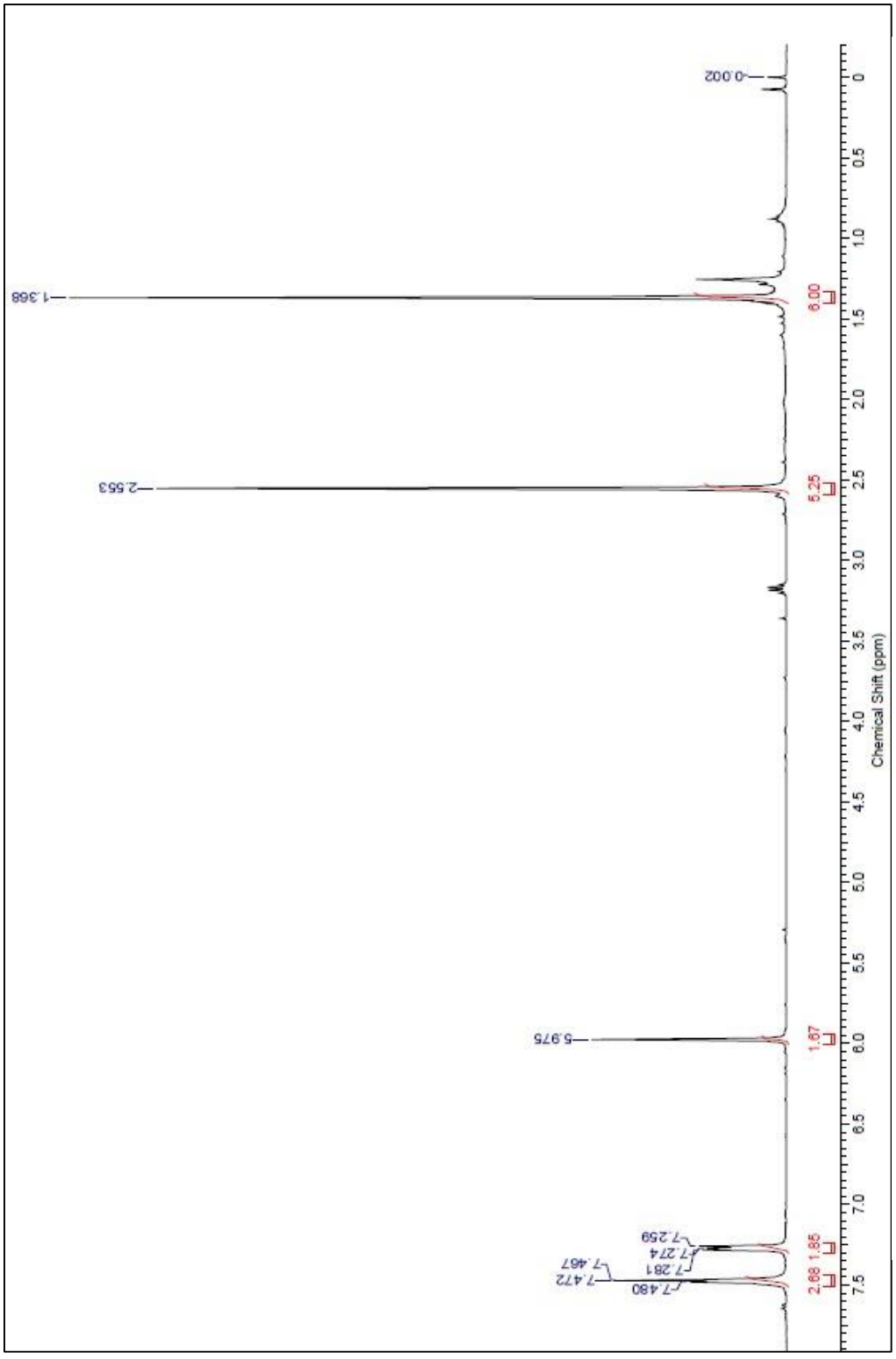

Figure A.1. ^{1} H NMR of 5,5-difluoro-1,3,7,9-tetramethyl-10-phenyl-5H-dipyrrolo[1,2-c:2',1'-f][1,3,2]diazaborinin-4-ium-5-uide

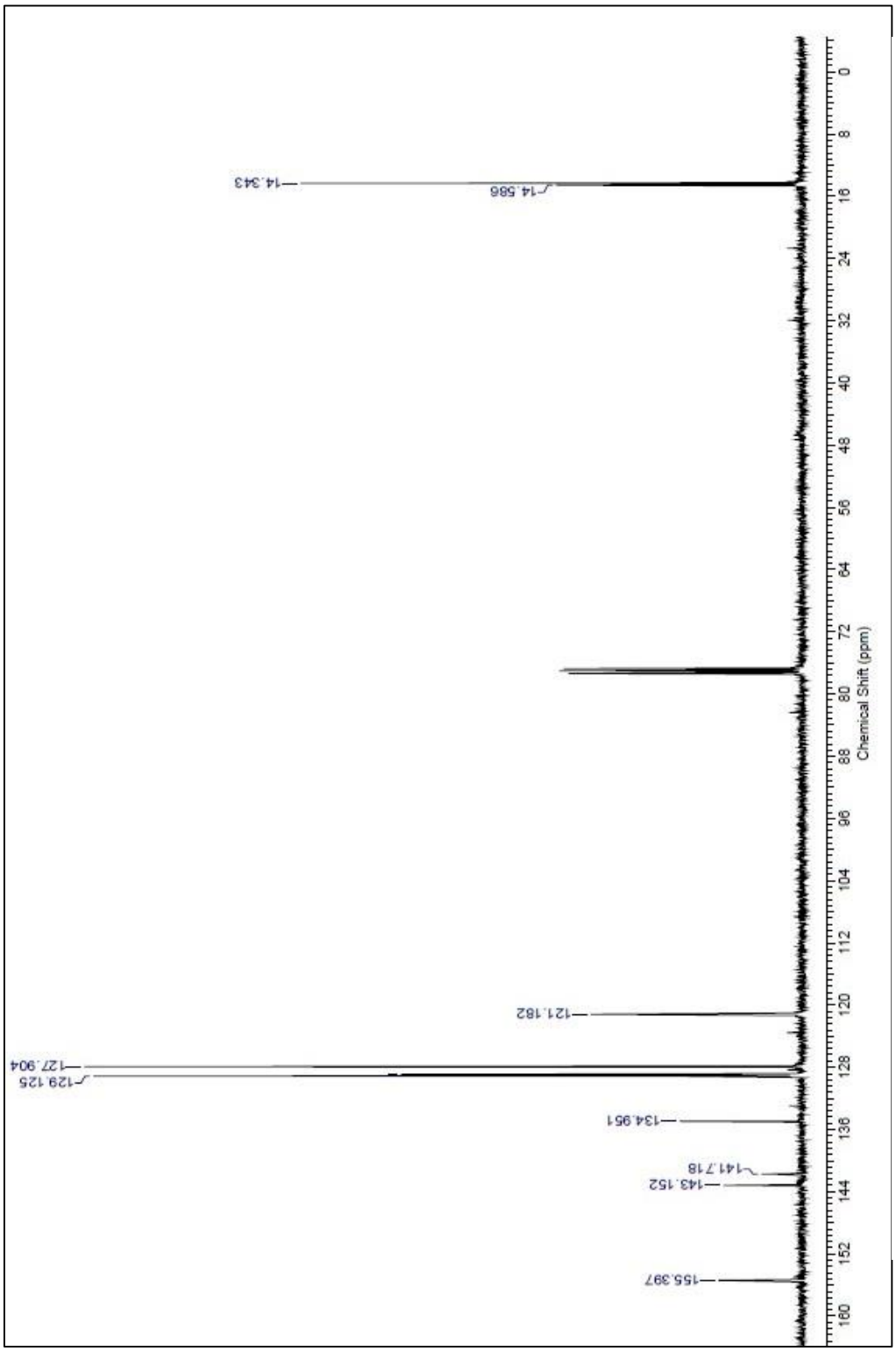

Figure A.2. ^{13}C NMR of 5,5-difluoro-1,3,7,9-tetramethyl-10-phenyl-5H-dipyrrolo[1,2-c:2',1'-f][1,3,2]diazaborinin-4-ium-5-uide

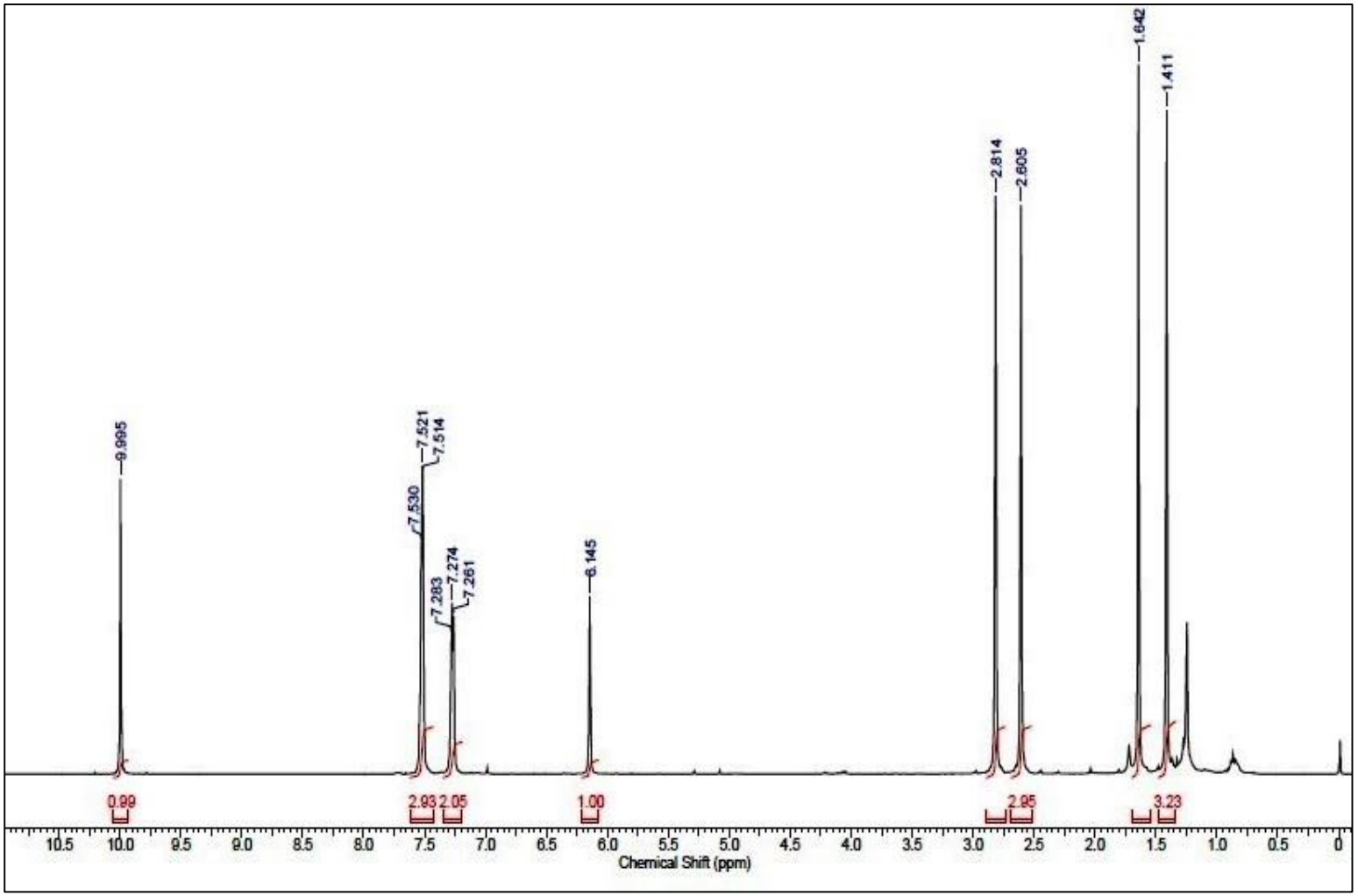

Figure A.3. ^{1}H NMR of 5,5-difluoro-8-formyl-1,3,7,9-tetramethyl-10-phenyl-5H-dipyrrolo[1,2-c:2',1'-f][1,3,2]diazaborinin-4-ium-5-uide

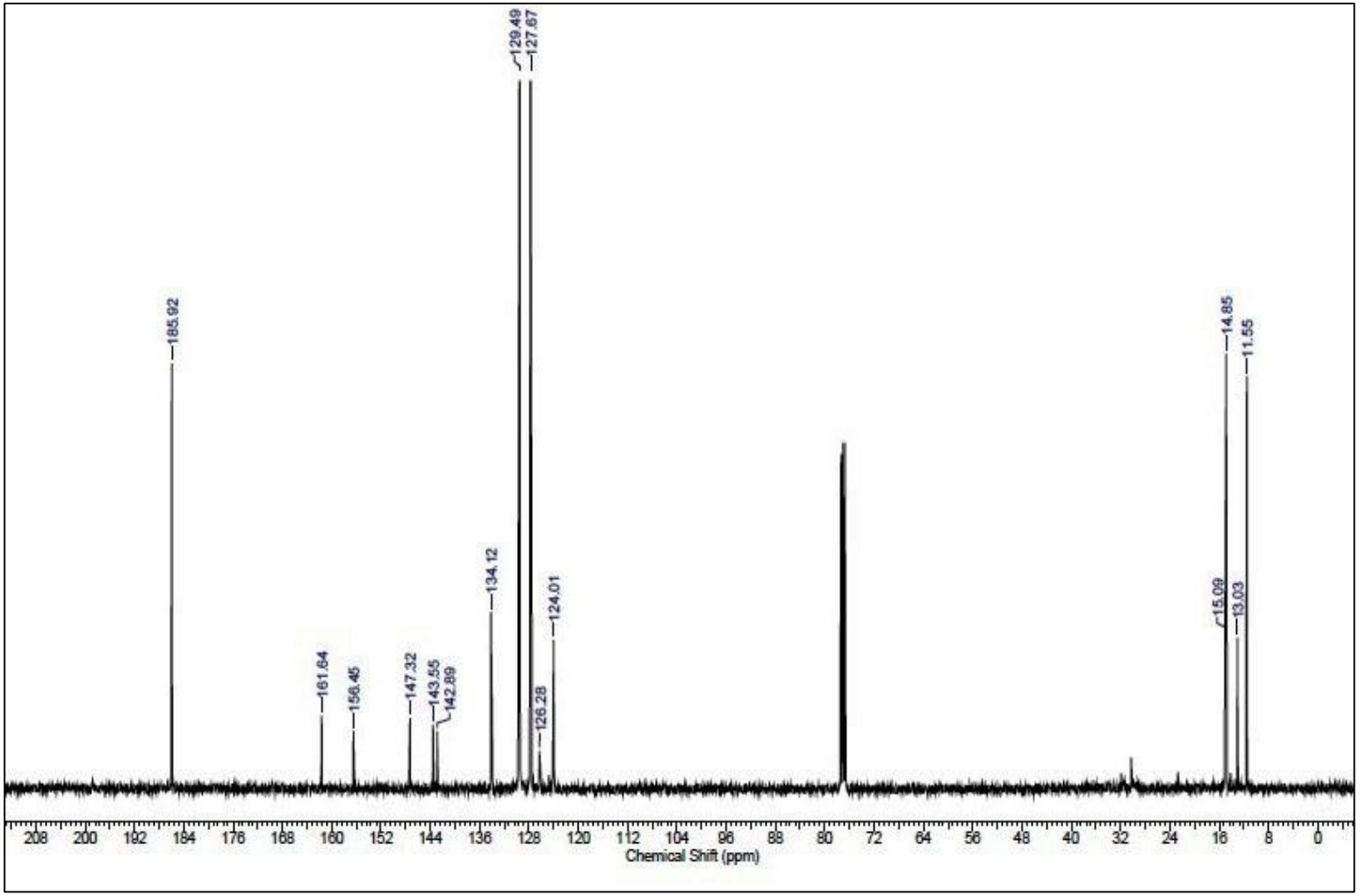

Figure A.4. ^{13}C NMR of 5,5-difluoro-8-formyl-1,3,7,9-tetramethyl-10-phenyl-5H-dipyrrolo[1,2-c:2',1'-f][1,3,2]diazaborinin-4-ium-5-uide

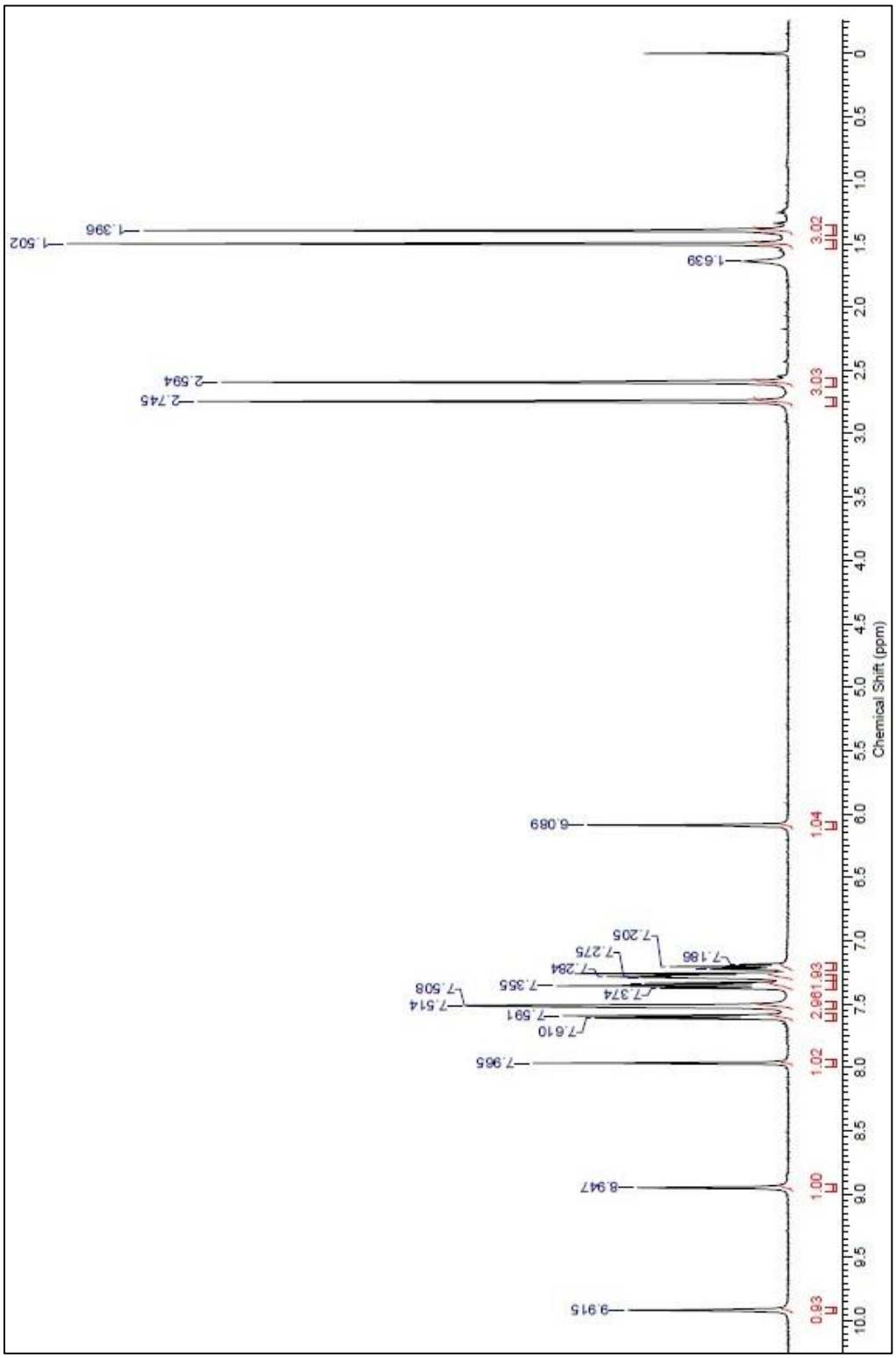

Figure A.5. ^{1}H NMR of (E)-5,5-difluoro-1,3,7,9-tetramethyl-10-phenyl-8-((2-(phenylcarbamothioyl)hydrazono)methyl)-5H-dipyrrolo[1,2-c:2',1'-f][1.3.2]diazaborinin-4-ium-5-uide

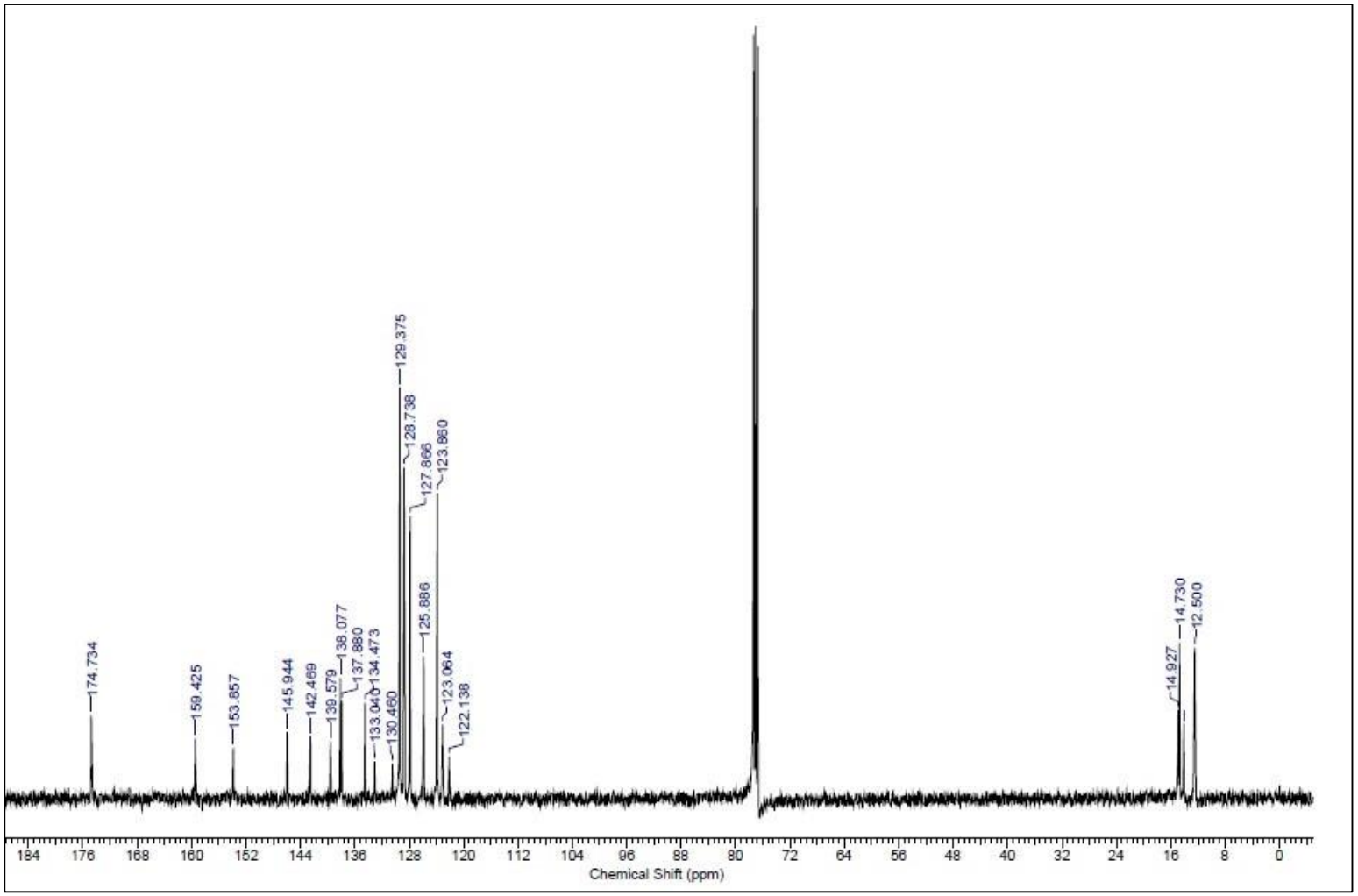

Figure A.6. ^{13}C NMR of (E)-5,5-difluoro-1,3,7,9-tetramethyl-10-phenyl-8-((2-(phenylcarbamothioyl)hydrazono)methyl)-5H-dipyrrolo[1,2-c:2',1'-f][1.3.2]diazaborinin-4-ium-5-uide

APPENDIX B

MASS SPECTRA OF COMPOUNDS

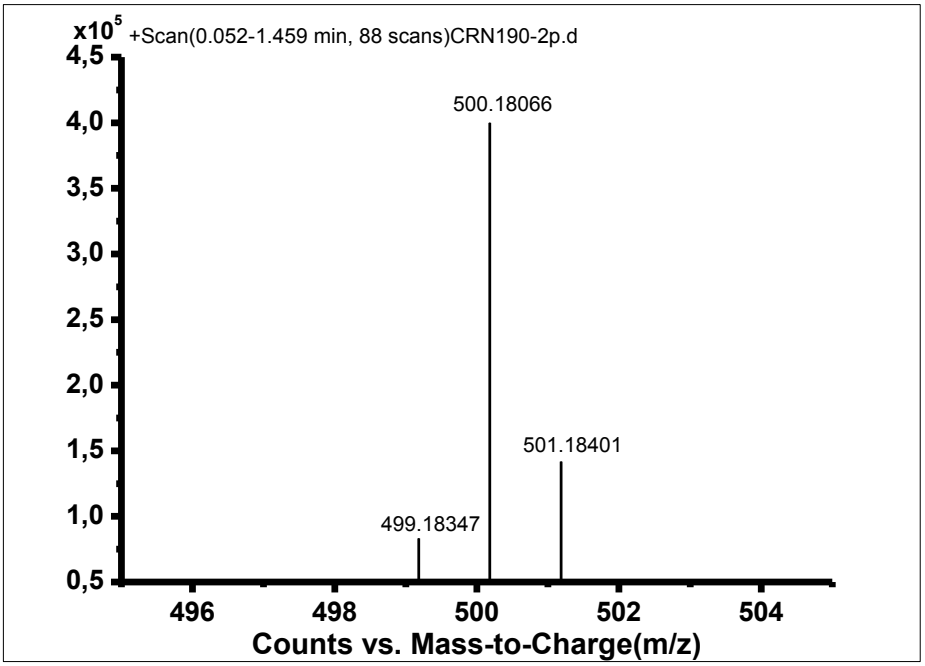

Figure B.1. Mass Spectrum of (E)-5,5-difluoro-1,3,7,9-tetramethyl-10-phenyl-8-((2-(phenylcarbamothioyl)hydrazono)methyl)-5H-dipyrrolo[1,2-c:2',1'-f][1,3,2]diazaborinin-4-ium-5-uide

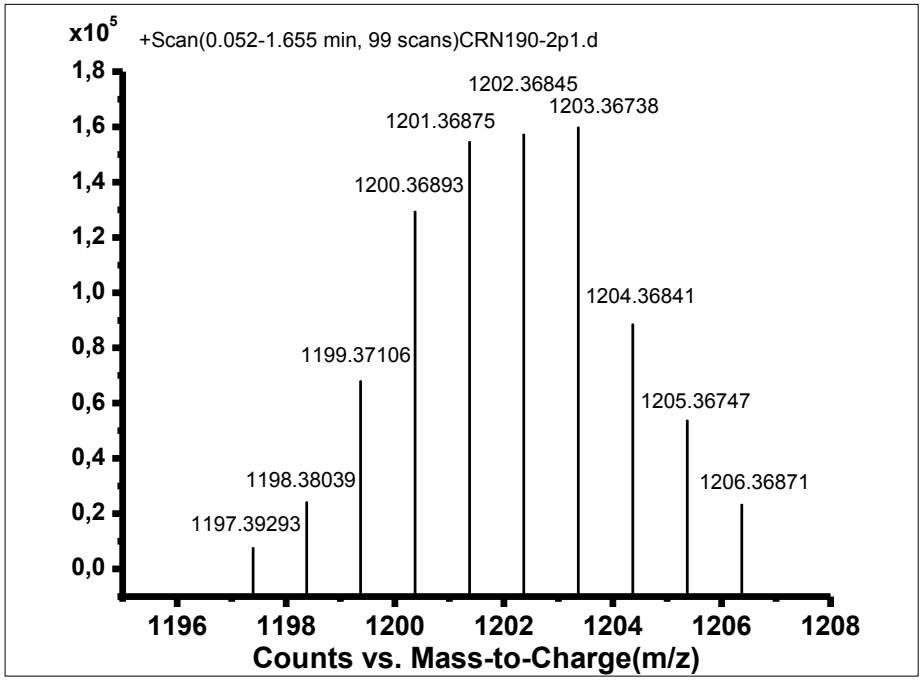

Figure B.2. Mass Spectrum of the Obtained Hg-Sensor Complex